# An innate defense peptide BPIFA1/SPLUNC1 restricts influenza A virus infection

# An innate defense peptide BPIFA1/SPLUNC1 restricts influenza A virus infection

Khondoker M. Akram[1¶], Nathifa A. Moyo[2¶], Gail H. Leeming[2,3], Lynne Bingle[4], Seema Jasim[5], Saira Hussain[5], Anita Schorlemmer[6], Anja Kipar[2,3,7], Paul Digard[5], Ralph A. Tripp[8], Ralph V. Shohet[6], Colin D. Bingle[1&], James P. Stewart[2*&]

[1]Academic Unit of Respiratory Medicine, Department of Infection, Immunity and Cardiovascular Disease, University of Sheffield, Sheffield, UK
[2]Department of Infection Biology and [3]Veterinary Pathology, University of Liverpool, Liverpool, UK
[4]Academic Unit of Oral and Maxillofacial Pathology, School of Clinical Dentistry, University of Sheffield, Sheffield, UK
[5]The Roslin Institute, University of Edinburgh, Edinburgh, UK.
[6]John A. Burns School of Medicine**,** University of Hawaii**,** Honolulu, HI, USA.
[7]Institute of Veterinary Pathology, Vetsuisse Faculty, University of Zurich, Zurich, Switzerland
[8]Department of Infectious Diseases, University of Georgia, Athens, GA, USA.

**[*]Corresponding Author:**
James P. Stewart, Ph.D., Department of Infection Biology, The University of Liverpool, Liverpool Science Park IC2, 146 Brownlow Hill, Liverpool L3 5RF, UK
Tel: +44 151 795 0221
Email: j.p.stewart@liverpool.ac.uk (JPS)

¶ These authors contributed equally to this manuscript

& CDB and JPS are Joint Senior Authors

The authors declare that there are no conflicts of interest

## Abstract

The airway epithelium secretes proteins that function in innate defense against infection. BPI fold-containing family member A1 (BPIFA1) is secreted into airways and has a protective role during bacterial infections, but it is not known whether it also has an antiviral role. To determine a role in host defense against influenza A virus (IAV) infection and to find the underlying defense mechanism we developed transgenic mouse models that are deficient in BPIFA1 and used these, in combination with *in vitro* 3D mouse tracheal epithelial cell (mTEC) cultures, to investigate its antiviral properties. We show that BPIFA1 has a significant role in mucosal defense against IAV infection. BPIFA1 secretion was highly modulated after IAV infection. Mice deficient in BPIFA1 lost more weight after infection, supported a higher viral load and virus reached the peripheral lung earlier, indicative of a defect in the control of infection. Further analysis using mTEC cultures showed that BPIFA1-deficient cells bound more virus particles, displayed increased nuclear import of IAV ribonucleoprotein complexes and supported higher levels of viral replication. Our results identify a critical role for BPIFA1 in the initial phase of infection by inhibiting the binding and entry of IAV into airway epithelial cells.

## Introduction

The airway epithelium has a fundamental role in the initial defense against pathogens and as such secretes a number of proteins/peptides that function in innate defense [1]. Bactericidal/permeability-increasing (BPI) fold-containing family A1 (BPIFA1; also called SPLUNC1) is a glycoprotein that is highly expressed in the respiratory epithelium and submucosal glands of the upper airways in mice and humans [2-9]. The mouse and human BPIFA1 sequences are homologous [8, 10, 11]. Previous studies have demonstrated that BPIFA1 acts as a surfactant [12], can regulate the amiloride-sensitive epithelial sodium channel, ENaC [13] and affects mucociliary clearance in the upper airways [14]. It has also been shown to have anti-bacterial roles. For example, *Bpifa1* expression is induced after *Mycoplasma* infection, enhancing IL-8 production and bacterial clearance [15]. BPIFA1 also has a role in defense against *Klebsiella pneumoniae* [16], possibly acting through modulation of macrophage function [17]. Less is known about any anti-viral role of BPIFA1, although our previous work has shown modulation of BPIFA1 levels after murine γ-herpesvirus 68 infection [18].

Influenza A virus (IAV) is an enveloped RNA virus of the Orthomyxovirus genus. Seasonal influenza is a major cause of respiratory infection resulting in substantial morbidity, mortality and thus economic burden worldwide [19]. Pandemic influenza strains emerge sporadically as a result of genetic reassortment and are a substantial global health concern [20]. There are vaccines and antiviral drugs to combat influenza. However, due to rapid virus evolution, vaccines need to be re-formulated and re-administered most years [21] and resistance against antiviral drugs is emerging [22]. It is therefore important to understand how intrinsic and innate

mechanisms modulate influenza virus infection and how these may be used to develop novel therapeutic interventions.

The negative-sense, single-stranded genome of IAV comprises eight segments of viral RNA which are separately encapsidated into ribonucleoprotein particles (RNPs) [23]. Infection and entry of IAV into cells involves viral attachment, via the hemagglutinin (HA) glycoprotein that is embedded in the virion membrane, to cell surface receptors that contain sialic acid [24]. After binding, virus particles enter the cell by receptor-mediated endocytosis. Fusion of the virus membrane with the endosomal membrane results in release of RNPs into the cytoplasm [24, 25] which are then imported into the nucleus , where genome replication and transcription of viral genes take place [26]. Understanding the entry process and how the host counters it is critical to uncovering inhibitors with therapeutic potential.

In this study, we used transgenic mouse models combined with *in vitro* 3D-culture systems to show that BPIFA1 has a role in the intrinsic defense against IAV infection.

## Results

### BPIFA1 expression after IAV infection.

To determine changes in BPIFA1 levels following IAV infection, C57BL/6J mice were infected intranasally (i.n.) with $10^3$ pfu IAV X-31 (or as controls with *u.v.*-inactivated virus or mock-infected) and analyzed at time-points post-infection (p.i.). IAV X-31 is a mouse-adapted H3N2 strain that generates a sub-lethal infection [27]. It thus models most of the IAV-associated disease in humans and also allows for analysis over an extended time-course.

Firstly, levels of BPIFA1 in broncho-alveolar lavage (BAL) were accurately quantified using (Wes™; ProteinSimple). The results (Fig. 1) showed BPIFA1 levels decreased dramatically after infection (100-fold) to a nadir at day 7 p.i. before returning to a level that was not significantly different to uninfected mice by day 14 p.i. *u.v.*-inactivated virus did not affect the levels of BPIFA1 as measured at day 5 p.i.

Next, the pattern and quantity of BPIFA1 staining was determined by immunohistology (IH). In mock-infected mice, BPIFA1 was abundant in the epithelium of the trachea and bronchi (Fig. 2A, B arrows) but present only within scattered cells in the bronchioles (Fig. 2C, arrows) and absent in the surrounding alveoli (Fig. 2C). Following infection with IAV, a substantial decrease in the number of BPIFA1-positive cells was observed and confirmed by the quantitative analysis that showed a 4 – 8-fold ($p$ <0.05) decrease in the percentage area stained in the trachea and bronchi respectively to day 7 p.i.; at this point, there were foci of erosion with reduced cell height, loss of cilia, loss of cellular polarity and occasional loss of epithelial cells. Recovery of levels of BPIFA1 and evidence of epithelial regeneration with foci of multilayered epithelium and mitoses was seen by day 14 p.i. (Fig. 2A, B). The intensity of BPIFA1 staining in the positive areas (i.e. in individual epithelial cells) did not decrease significantly in the trachea, but in the bronchi a similar pattern to that of area stained was noted with an initial decrease followed by a gradual recovery. In contrast, in bronchioles the intensity of staining in epithelial cells increased five-fold to day 14 p.i., whilst the number of positive cells (area stained) increased three-fold by day 14 p.i. (Fig. 2C).

**Mice deficient in BPIFA1 support higher levels of IAV replication.**

To determine the role of BPIFA1 in defense against IAV, BPIFA1-deficient mice (*Bpifa1*$^{-/-}$) were generated as described in supplementary data and S1 Fig. (A). *Bpifa1*$^{-/-}$ mice expressed no detectable BPIFA1 protein in the lungs (S1 Fig. (B)), but did not exhibit any morphological changes or altered distribution of cell types in airways and alveoli (S1 Fig. (C); described in supplementary data).

C57BL/6J and *Bpifa1*$^{-/-}$ mice were infected i.n. with $10^3$ pfu IAV X-31. The weight of the mice and lung virus titers were determined over a 28-day period. The results (Fig. 3A, B) showed that *wt* mice were readily infected with IAV. They lost weight (max. 5%; day 6 p.i.) before recovering. Titers of IAV increased in the lungs, peaking at $10^6$ pfu/g tissue on day 5 p.i. Infection in *Bpifa1*$^{-/-}$ mice followed a similar course. Weight loss was significantly greater ($p < 0.01$) in *Bpifa1*$^{-/-}$ mice (12% at day 6 p.i.). In addition, IAV titers were significantly ($p < 0.05$) and at least 1 $\log_{10}$ higher at all time-points. Virus was not detectable in either group at days 7 and 14 p.i.

To control for potential developmental adaptation in the knockout mice, a club cell-specific, tamoxifen (tmx)-inducible conditional knockout mouse strain (*Bpifa1*$^{loxP}$; *Scgb1a1-CreER*$^{TM}$) was generated as described in the S1 text. Western blot analysis of lung tissue confirmed a 9-fold knockdown in the level of BPIFA1 in *Bpifa1*$^{loxP}$; *Scgb1a1-CreER*$^{TM}$ mice after tmx treatment as compared with mice that were treated with carrier (Fig. 3C).

*Bpifa1*$^{loxP}$; *Scgb1a1-CreER*$^{TM}$ mice were treated with either carrier (vegetable oil) or tmx and, along with untreated *Bpifa1*$^{loxP}$; *Scgb1a1-CreER*$^{TM}$ and *Bpifa1*$^{-/-}$ mice, were infected i.n. with IAV. Virus titers in the lungs were determined at day 7 p.i. The results (Fig. 3D) showed that titers of infectious virus were significantly lower in untreated or carrier-treated mice than in tmx-treated *Bpifa1*$^{loxP}$; *Scgb1a1-CreER*$^{TM}$

mice or *Bpifa1*$^{-/-}$ mice. Thus, reduction of BPIFA1 expression using either total or conditional knockout of BPIFA1 enabled IAV to be more pathogenic and replicate to higher titers in the lungs of infected mice.

**BPIFA1 limits the initial spread of IAV *in vivo*.**

To assess whether BPIFA1 influenced the distribution of IAV infection, C57BL/6J and *Bpifa1*$^{-/-}$ mice were infected and IAV-infected cells identified by IH. At day 1 p.i., IAV antigen was seen within, and adjacent to foci of necrotic respiratory epithelial cells in the nasal cavity, trachea, bronchi and proximal bronchioles of both *wt* and *Bpifa1*$^{-/-}$ mice (S2 Fig., arrows). However, in *Bpifa1*$^{-/-}$ mice, epithelial cells in the distal bronchioles were found to be infected and macrophages in alveoli around the infected bronchioles were positive for IAV (Fig. 4. arrows and red arrowheads respectively). In contrast, IAV antigen was not observed in distal bronchioles and alveoli of *wt* mice. At subsequent days post-infection there were no differences in the distribution of IAV antigen between *wt* and *Bpifa1*$^{-/-}$ mice.

Thus, in the absence of BPIFA1, IAV infection reached the distal airways and alveoli earlier during infection.

**BPIFA1 restricts IAV infection in normal epithelial cells.**

Given the differences in viral titer as early as day 1 p.i., we hypothesized that one function of BPIFA1 could be to influence directly the infection of epithelial cells. To investigate this, tracheal cell cultures were established from mice and cultured at the air-liquid interface to generate well-differentiated cultures (mTEC) [28, 29]. The validation of these cultures from *wt* mice is presented in supplementary data and S3 Fig. Differentiated mTEC ALI cultures displayed phenotypic features associated with

122 complex populations of cells including ciliated cells (β-tubulin, FoxJ1), BPIFA1,
123 mucin (MUC5B), and SCGB1A1 (CCSP)-expressing cells that matched with the
124 features of the native rodent airway epithelium. The cultures from *Bpifa1*$^{-/-}$ mice had
125 similar levels of ciliogenesis (β-tubulin staining) and mucin (MUC5B staining) to
126 those from *wt* counterparts (S4 Fig.). Quantification of β-tubulin-staining showed that
127 approx. 17% of cells were ciliated in both types of cultures. In *wt* cultures, 24% of
128 cells were BPIFA1 positive and were non-ciliated. Thus, mTEC ALI cultures are
129 highly representative of mouse airway epithelium and an ideal model to study the
130 role of BPIFA1 during infection.

131 mTEC ALI cultures from *wt* and *Bpifa1*$^{-/-}$ mice were infected with IAV (0.1
132 pfu/cell) and infection analyzed by immunofluorescence (IF). In *wt* mTEC ALI cells,
133 IAV antigen was observed predominantly in epithelial cells that did not express
134 BPIFA1, at both 24 and 48 h p.i. (Fig. 5B, C). An increased number of cells
135 containing IAV NP antigen was seen in *Bpifa1*$^{-/-}$ mTEC ALI cultures as compared
136 with *wt* cells at both time-points (Fig. 5E, F). Quantification revealed a >2-fold and
137 nearly 2-fold higher intracellular IAV NP load in *Bpifa1*$^{-/-}$ than in *wt* mTEC cultures at
138 24 h p.i. and 48 h p.i. respectively (Fig. 5G; $p < 0.05$). There was also a significant
139 increase in infectious IAV titer in apical wash fluid from *Bpifa1*$^{-/-}$ compared with *wt*
140 cells (Fig. 5H). Thus, BPIFA1 inhibits the infection of normal (mTEC ALI) cells by IAV
141 at a stage up to or before early viral gene expression.

142

143 **BPIFA1 limits the import of IAV into epithelial cells.**

144 Import of virus ribonucleoprotein (vRNP) complexes into the nucleus is one of the
145 initial steps of the IAV replication cycle. To investigate whether BPIFA1 influences
146 the early stages of IAV infection, day 14 mTEC ALI cultures were infected with IAV.

147 Import of RNP complexes into the nucleus was then assessed by
148 immunofluorescence analysis using anti-IAV NP. Blocking protein synthesis with
149 cycloheximide (CHX) was performed to distinguish imported RNPs from *de novo* NP
150 production. The amount of purified virus used was sufficient enable detection of RNP
151 import in 100% of cells in an equivalent assay performed on MDCK cells (data not
152 shown). The results (Fig. 6A, B) showed that in the absence of CHX, IAV NP was
153 readily observed 4 h after infection in the nuclei of cells from *wt* mice but, as with the
154 previous experiment, was present in 3.5x more nuclei in cells from *Bpifa1*$^{-/-}$ mice. In
155 the presence of CHX, RNP complexes were observed in the nuclei of 1% of *wt* cells
156 but in a significantly ($p < 0.05$) higher proportion (25x) of nuclei in *Bpifa1*$^{-/-}$ cells (Fig.
157 6A right panels, B, C). Thus BPIFA1 appreciably decreased the number of cells with
158 visible accumulation of IAV RNPs after infection, indicating that it acts at an early
159 stage of the viral life cycle.
160
161 **BPIFA1 inhibits IAV binding to respiratory epithelial cells.**
162 To determine if BPIFA1 affected virus binding, mTEC ALI cultures derived from
163 *Bpifa1*$^{-/-}$ and *wt* mice were incubated with Alexa Fluor 488-labelled IAV (IAV-488)
164 and bound virus was assessed by confocal microscopy. The amount of labelled virus
165 used was sufficient to enable detection of binding in 100% of cells in an equivalent
166 assay performed on MDCK cells (data not shown). *wt* cells showed IAV binding
167 predominantly to the surface of Foxj1-positive (ciliated) cells that were negative for
168 BPIFA1 (Fig. 7A). The BPIFA1-positive sub-population of cells (non-ciliated; S3 Fig.
169 A, C) presented as focal clusters in mTEC ALI cultures (outlined in yellow) and were
170 predominantly free from IAV-binding (Fig. 7A). Analysis of the distribution of α2,3-
171 linked and α2,6-linked sialic acid residues using the lectins MAA and SNA

172 respectively showed that there were numerous cells with α2,3-linked residues on the
173 cell surface in both *wt* and *Bpifa1*$^{-/-}$ cultures (mean *n* = 3; 25% and 22% respectively)
174 and that these were on the BPIFA1-negative cells (S5 Fig. (A)). The few α2,6-
175 positive cells present in the *wt* and *Bpifa1*$^{-/-}$ cultures (mean *n* = 3; 3% and 5%
176 respectively) were mostly BPIFA1-positive (S5 Fig. (B - E)). Quantification of bound
177 IAV-488 showed that the integrated fluorescence intensity from *Bpifa1*$^{-/-}$ cells was 4
178 fold greater than that from *wt* cells (Fig. 7B, C). Thus, our data show that IAV bound
179 predominantly to ciliated cells that were BPIFA1-negative, α2,3-linked sialic acid-
180 positive, and that the presence of BPIFA1 decreased the binding of IAV to these
181 cells.
182

## Discussion

BPIFA1 is constitutively expressed and secreted by the airway epithelium [2, 6, 7, 18, 30, 31] including the submucosal glands [9, 28, 30, 31]. However, its precise biological functions remain elusive. Our studies have uncovered an important role for BPIFA1 in the host defense against IAV infection. BPIFA1 levels were modulated after infection and genetic knockout of BPIFA1 led to a higher viral titer both *in vivo* and in mTEC ALI cultures. There was also greater nuclear import of virus RNP complexes and binding of virus to cells in mTEC cultures lacking BPIFA1.

BPIFA1 has previously been shown to have a defensive role in *M. pneumoniae* and *K. pneumoniae* infection, enhancing bacterial clearance and inhibiting biofilm formation [15, 16]. Here we show for the first time, that BPIFA1 also has a major role in the defense against IAV. Notably higher weight loss was observed and higher viral titers (> 1 $\log_{10}$) were recovered from the lungs of *Bpifa1*$^{-/-}$ mice as compared to *wt* controls. A more rapid spread of IAV to the lung parenchyma was also seen in *Bpifa1*$^{-/-}$ mice. Specifically, IAV antigen was observed in the bronchiolar epithelium and alveoli of *Bpifa1*$^{-/-}$ but not of *wt* mice at 24 h p.i. indicating a possible role for BPIFA1 both in intrinsic or innate defense during early infection and in the adaptive immune response to IAV. The higher viral titers in lungs after conditional knockdown of BPIFA1 in *Scgb1a1*-expressing club cells indicates that the observations seen in the *Bpifa1*$^{-/-}$ mice are not due to developmental adaptations to the total loss of BPIFA1 expression.

To investigate intrinsic functions of BPIFA1 in the airway epithelium we cultured mTEC cells from *wt* and *Bpifa1*$^{-/-}$ mice. Although we did not formally rescue the *Bpifa1*$^{-/-}$ cells using exogenous protein, we controlled for differences between

cultures by performing extensive phenotypic characterization. Thus, approximately 25% of the cells in *wt* mTEC had α2,3-linked sialic acid (SA) residues on the surface. These cells were BPIFA1-negative. A similar proportion of cells (22%) were α2,3 SA-positive in the *Bpifa1*$^{-/-}$ cultures. Very few cells on *wt* and *Bpifa1*$^{-/-}$ cultures were α2,6 SA-positive (3% and 5% respectively). Mouse-adapted IAV strains such as those used in this study (X-31 and PR8) will use both α2,3- and α2,6-linked and sialic acid residues as a receptor [32, 33]. The similar proportions of cells with α2,3- and α2,6-linked and sialic acid residues between *wt* and *Bpifa1*$^{-/-}$ cultures indicates that differences in infection and binding between *wt* and *Bpifa1*$^{-/-}$ are due to the absence or presence of BPIFA1 and not differences in the number of cells expressing receptors. Infection of mTEC cultures with IAV paralleled our observations *in vivo* in that there was a significantly more rapid spread and higher viral titers in cultures lacking BPIFA1. In line with the distribution of α2,3-linked sialic acid receptors, IAV had a preference for infecting the BPIFA1-negative population. This confirms a role for BPIFA1 in the intrinsic defense against IAV at the airway epithelium during the first few days of infection and shows that the secreted protein exerts its effects on the epithelial cell surface rather than solely in the cells that produce it.

Further analysis revealed a much greater import of IAV RNPs into the nuclei of cells and significantly increased virus binding in the *Bpifa1*$^{-/-}$ cultures. The fact that only a percentage of cells were infected in these assays reflects in part the complex nature of mTEC ALI cultures and where only a proportion of the cells express the α2,3- and α2,6-SA receptors. The greater level of inhibition in the RNP import assay compared to the binding assay suggests an important role for BPIFA1 in decreasing post-binding entry into cells via endosomes as well as initial binding of IAV to normal ciliated epithelial cells in airways. BPIFA1 is secreted and is present in the periciliary

233 layer [34] so it is easy to envisage how it might be part of a barrier to IAV infection at
234 the epithelial surface. We did not characterize whether and how BPIFA1 binds to
235 virus particles. However, BPIFA1 could either form a non-specific barrier to IAV
236 engaging with cellular receptors, or bind to IAV and prevent receptor interactions.
237 Gel-forming mucins such as MUC5AC inhibit virus infection [35] and BPIFA1 has been
238 shown to associate with the mucus rich portion of the pericellular lining fluid [34, 36]. It
239 has been hypothesized that in the case of IAV this is due to competitive inhibition for
240 receptors as MUC5AC from mice contains abundant α2,3-linked sialic acid residues
241 [35]. The glycosylation on BPIFA1 contains sialic acid residues [37] and could potentially
242 act by binding to IAV particles via specific sialic acid-HA interactions. Alternatively,
243 BPIFA1 is a member of the wider tubular lipid-binding (TULIP) superfamily [38], has a
244 hydrophobic cavity and binds several lipids found in mammalian membranes [39]. It
245 therefore has the potential to bind to lipids found in the IAV membrane and interfere
246 with receptor binding and endosomal fusion. Further studies are required to
247 determine precisely how BPIFA1 blocks binding and entry of IAV into normal
248 epithelial cells.

249 Previous studies have shown that infection by a number of pathogens (e.g. *P.*
250 *aeruginosa*, *S. pneumoniae, M. pneumoniae,* murine γ-herpesvirus 68 and IAV)
251 cause an initial transient increase in secretion of the protein in the first 2 - 3 hours
252 post infection but this is followed by a decrease over 2 - 7 days [15, 18, 40]. Our results *in*
253 *vivo* extend these observations using IAV (Figs. 1 - 2). Decrease in BPIFA1 levels
254 after infection is mediated by pathogen-associated molecular patterns (PAMPs) and
255 IFN-γ [40]. The IAV strains used here target BPIFA1-negative ciliated epithelial cells
256 and BPIFA1 is produced by non-ciliated epithelial cells. Thus, although IAV induces
257 necrosis of respiratory epithelial cells, the decrease in BPIFA1 expression is unlikely

result from direct killing of BPIFA1-expressing cells. Also, intact respiratory epithelia exhibited decreased BPIFA1 expression at day 7 p.i. (Fig. 2). IAV induces signaling by a number of PAMPs and so the decrease in BPIFA1 could be due to this mechanism [41]. Inactivated IAV had no effect suggesting that active replication is required to mediate a decrease in BPIFA1 levels. After resolution of the initial infection, BPIFA1 levels returned to pre-infection levels in BAL and the tracheal and bronchial epithelium.

It seems unlikely that BPIFA1 has evolved to have a role in the defense against IAV alone and thus it is likely that the protein will influence the pathogenesis of other viruses. It has been shown to have an inhibitory effect on the replication of Epstein-Barr virus (a membrane-bound herpesvirus) in lymphoblastoid cells [42]. Down-regulation of BPIFA1 expression [43] and polymorphisms in the BPIFA1 gene are also associated with susceptibility to Epstein-Barr virus-associated nasopharyngeal carcinoma [44]. It will be of interest to determine if BPIFA1 affects the pathogenesis of other respiratory viruses.

These studies have uncovered a significant and unappreciated role for BPIFA1 in host defense against experimental IAV infections in murine models. It remains to be seen if this protein is able to modulate IAV infection in the human host in a similar manner. The observation of elevated levels of BPIFA1 in nasal aspirates of children with IAV [45] suggests that some modulation of the protein does occur during clinical infection and thus is a potential biomarker. We propose that BPIFA1 may be one component of the airway surface lining fluid critical to antiviral host defense. Further studies are needed to determine if natural variations in BPIFA1 levels due to genetic polymorphisms [44] may pre-dispose to more severe IAV-associated disease.

283

## Methods

**Virus.**

Influenza virus strains A/X-31 (X-31, H3N2) and A/PR/8/34 (PR8, H1N1) were propagated in the allantoic cavity of 9-day-old embryonated chicken eggs and titered by plaque assay on MDCK cells [46].

**Mice**.

Animal work was reviewed and approved by the local University of Liverpool Animal Welfare Committee and performed under UK Home Office Project Licences 40/2483 and 70/8599. Mice were all specified pathogen free and maintained under barrier conditions in individually ventilated cages. Transgenic *Bpifa1*$^{-/-}$ mice were bred at the University of Liverpool under UK Home Office Project Licence 70/8378. Transgenic mice deficient in BPIFA1 (*Bpifa1*$^{-/-}$) and conditional knockout were generated (*Bpifa1*$^{loxP}$; *Scgb1a1-CreER*$^{TM}$) as described in S1 text and S1 Fig. Both transgenic strains were backcrossed 10 generations to C57BL/6J. Wild-type sex and age-matched C57BL/6J control mice were purchased from Charles River (UK).

**Tamoxifen Administration**.

A 20 mg/ml Tamoxifen (tmx) stock solution was dissolved in Mazola corn oil. Tmx was administered by gavage of 0.25 mg per gram body weight to *Bpifa1*$^{loxP}$; *Scgb1a1-CreER*$^{TM}$ adults daily for five days. Mice were then infected with IAV 4 days after the last gavage.

**Virus infection of mice.**

Animals were randomly assigned into multiple cohorts, anesthetized lightly with KETASET i.m. and inoculated intra-nasally with $10^3$ pfu IAV in 50 µl sterile PBS, or were mock-infected with a similar volume of allantoic fluid. Mice were sacrificed at

variable time-points after infection by cervical dislocation. Tissues were removed immediately for downstream processing.

**Histology, Immunohistology.**

Histology and immunohistology (IH) was performed on paraformaldehyde-fixed, paraffin-embedded tissue using the peroxidase anti-peroxidase (PAP) method as previously described [47, 48]. Primary antibodies used were rabbit anti-mBPIFA1 [6] and goat anti-IAV (Meridian Life Sciences Inc., B65141G).

**Quantitative Histopathological Assessment.**

The percentage area and density of DAB staining within airway epithelium was quantified using whole slide images scanned and analyzed using Image-Pro Premier image analysis software version 9.1 (MediaCybernetics Inc.). An automated macro and app (named Trachea.ipp and Airways.ipx, respectively) were developed in conjunction with MediaCybernetics Inc. They were designed to identify and outline regions of interest comprising the airway epithelium of the trachea, bronchi and bronchioles, while excluding other cells. The macro and app analyze thresholds of hue, luminosity and saturation, which were set relative to the chromogen (DAB) utilized for BPIFA1 localization. These data provided an average density of staining for each region of interest. The percentage area stained was defined as the brown area (positive immunostaining) divided by the total brown area plus blue area (hematoxylin; negative staining) ×100.

**Western Blotting.**

Samples were analysed by 12.5% SDS-PAGE gel electrophoresis and blotted using rabbit anti-mBPIFA1 [6]. Band density was measured using the gel analysis tool of Image J software.

**Quantitative protein analysis.**

The Wes™ system was used to identify and quantify BPIFA1 protein in BAL and lung samples (ProteinSimple) and rabbit anti-mBPIFA1 as primary antibody. The area of BPIFA1 peak, in relation to the standard curve, was determined and virtual blot-like images generated using Compass software (ProteinSimple).

**Mouse tracheal epithelial cell cultures.**

Mouse tracheal epithelial cells (mTEC) were isolated and differentiated into upper airway-like epithelium in an air-liquid interface (ALI) culture following previously described methodology with slight modification [28, 29]. Whole tracheas were excised from 6-8 weeks old mice. Five or six tracheas were pooled for each evaluation.

**Immunofluorescent labeling and confocal imaging.**

Transwell membranes were fixed with 10% buffered formalin and then stained using primary and secondary antibodies. Primary antibodies used were as follows: rabbit anti-BPIFA1 (1:200)[6], rabbit anti-LPLUNC1 (1:100)[6], mouse anti-β tubulin (1:100; Sigma Aldrich, Cat No- T5201), mouse anti-Foxj1 (1:100; eBioscience, Cat No- 14-9965-82, Clone- 2A5), goat anti-SCGB1A1 (1:500; Gift from Barry Stripp), rabbit anti-MUC5B (1:100; Santa Cruz; H-300, Cat no- sc-20119,) and mouse anti-Influenza A virus NP (anti-IAV NP; 1:200; H16-L10-4R5 (ATCC® HB-65™)). Secondary antibodies are as follows (all from Life Technology; 1:200): Alexa Fluor 568 Goat anti-rabbit antibody (Cat No- A11011), Alexa Fluor 488 Goat anti-mouse antibody (Cat No- A11001), Alexa Fluor 488 Rabbit anti-goat antibody (Cat No- A11078), Alexa Fluor 633 Goat anti-mouse IgG (Cat No- A21050). Samples were mounted on glass slides with DAPI Vectashield (Vector Laboratories, Cat No- H-1200) and visualized with an Olympus Fluoview 1000 Confocal microscope.

**Virus labeling and IAV binding assay.**

IAV A/PR/8/34 was purified from the allantoic fluid of infected eggs by pelleting

through a 30% sucrose/PBS cushion followed by banding on 15-60% sucrose/PBS density gradients. Virus was then labelled using a green Alexa-fluorophore labelling kit (Life Technologies) to yield Alexa Fluor 488-labelled virus (IAV-488). Unreacted dye was removed by pelleting the virus at 125,000 *g*. For binding assays, IAV-488 was added to the apical surfaces of day 14 mTEC ALI cultures. After incubation for 1 h and washing off unbound virus, membranes were immediately fixed with 10% buffered formalin and co-stained with anti-BPIFA1 and anti-FoxJ1 antibodies. Images were captured from at least five fields per sample by confocal microscope. Integrated fluorescence intensity was measured by Image J to assess the levels of IAV-488 binding on the cell surface of mTEC cultures. Three independent experiments were conducted with cells from three different batches of mice.

**Nuclear import assay of IAV ribonucleoprotein (vRNP) complexes.**

Apical surfaces of Day 14 ALI mTEC cultures were infected with purified IAV A/PR/8/34. Following infection, cells were overlaid with DMEM/F-12 media plus/minus cycloheximide (CHX) at a final concentration of 100 μg/ml (no CHX was the control). Cells were incubated in 5% $CO_2$ at 37°C for 4 h, then washed three times with pre-warmed HBSS and fixed with 10% buffered formalin as above. Samples were processed and dual immunostained with anti-IAV NP as described above. Cells displaying nuclear localization of viral RNP were counted at 40x magnification in five fields (one center and four peripheral fields) per sample and presented as a percentage of positive cells over total cells counted. Three independent experiments were conducted with cells from three biologically different batches of mice.

## Acknowledgements.

This work was supported by Biotechnology and Biological Sciences Research Council (UK) grants BB/K009664/1 (to JPS, AK and GHL), BB/K009737/1 (CDB and LB), BBS/E/D/20241864 (PD) and the Georgia Research Alliance to RAT. The authors wish to thank Barry Stripp for the generous gift of anti-SCGB1A1 and Emma Rawlins for help and advice regarding the use of Scgb1a1-Cre mice and conditional KO mouse technology. Thanks are due to the technical staff in the Histology Laboratories, Veterinary Laboratory Services, School of Veterinary Science, University of Liverpool, for excellent technical assistance.

## Author contributions

CDB, LB, AK, RAT; planned the project, designed experiments and analyzed the data. JPS. planned the project, designed experiments, analyzed the data, interpreted results, and wrote the manuscript. RVS planned and designed the transgenic knockout strategies. KMA designed and performed the *in vitro* mTEC experiments, analysed data and interpreted the results. NAM designed and performed the *in vivo* experiments, analysed data and interpreted the results. AS generated the *Bpifa1*$^{loxP}$ and *Bpifa1*$^{-/-}$ transgenic mouse lines. SJ and SH helped perform the RNP import and binding assays. PD designed and interpreted the SNP import and binding assays. GHL performed and interpreted the histology and immunohistology examinations. All authors reviewed, revised, and approved the manuscript for submission.

## Disclosure

The Authors declare that there are no conflicts of interest

**REFERENCES.**


1. Whitsett JA, Alenghat T. Respiratory epithelial cells orchestrate pulmonary innate immunity. *Nat Immunol* 2015; **16**(1)**:** 27-35.

2. LeClair EE, Nguyen L, Bingle L, MacGowan A, Singleton V, Ward SJ *et al.* Genomic organization of the mouse plunc gene and expression in the developing airways and thymus. *Biochem Biophys Res Commun* 2001; **284**(3)**:** 792-797.

3. LeClair EE, Nomellini V, Bahena M, Singleton V, Bingle L, Craven CJ *et al.* Cloning and expression of a mouse member of the PLUNC protein family exclusively expressed in tongue epithelium. *Genomics* 2004; **83**(4)**:** 658-666.

4. Bingle CD, Craven CJ. PLUNC: a novel family of candidate host defence proteins expressed in the upper airways and nasopharynx. *Hum Mol Genet* 2002; **11**(8)**:** 937-943.

5. Bingle CD, Gorr SU. Host defense in oral and airway epithelia: chromosome 20 contributes a new protein family. *Int J Biochem Cell Biol* 2004; **36**(11)**:** 2144-2152.

6. Musa M, Wilson K, Sun L, Mulay A, Bingle L, Marriott HM *et al.* Differential localisation of BPIFA1 (SPLUNC1) and BPIFB1 (LPLUNC1) in the nasal and oral cavities of mice. *Cell Tissue Res* 2012; **350**(3)**:** 455-464.

7. Weston WM, LeClair EE, Trzyna W, McHugh KM, Nugent P, Lafferty CM *et al.* Differential display identification of plunc, a novel gene expressed in embryonic palate, nasal epithelium, and adult lung. *J Biol Chem* 1999; **274**(19)**:** 13698-13703.

8. Bingle CD, Bingle L. Characterisation of the human plunc gene, a gene product with an upper airways and nasopharyngeal restricted expression pattern. *Biochim Biophys Acta* 2000; **1493**(3)**:** 363-367.

9. Di YP, Harper R, Zhao Y, Pahlavan N, Finkbeiner W, Wu R. Molecular cloning and characterization of spurt, a human novel gene that is retinoic acid-inducible and encodes a secretory protein specific in upper respiratory tracts. *J Biol Chem* 2003; **278**(2)**:** 1165-1173.

10. Bingle CD, LeClair EE, Havard S, Bingle L, Gillingham P, Craven CJ. Phylogenetic and evolutionary analysis of the PLUNC gene family. *Protein Sci* 2004; **13**(2)**:** 422-430.

11. Bingle CD, Bingle L, Craven CJ. Distant cousins: genomic and sequence diversity within the BPI fold-containing (BPIF)/PLUNC protein family. *Biochem Soc Trans* 2011; **39**(4)**:** 961-965.

12. Gakhar L, Bartlett JA, Penterman J, Mizrachi D, Singh PK, Mallampalli RK *et al.* PLUNC is a novel airway surfactant protein with anti-biofilm activity. *PLoS One* 2010; **5**(2)**:** e9098.

13. Garcia-Caballero A, Rasmussen JE, Gaillard E, Watson MJ, Olsen JC, Donaldson SH *et al.* SPLUNC1 regulates airway surface liquid volume by protecting ENaC from proteolytic cleavage. *Proc Natl Acad Sci U S A* 2009; **106**(27)**:** 11412-11417.

14. McGillivary G, Bakaletz LO. The multifunctional host defense peptide SPLUNC1 is critical for homeostasis of the mammalian upper airway. *PLoS One* 2010; **5**(10)**:** e13224.

15. Chu HW, Thaikoottathil J, Rino JG, Zhang G, Wu Q, Moss T *et al.* Function and regulation of SPLUNC1 protein in Mycoplasma infection and allergic inflammation. *J Immunol* 2007; **179**(6)**:** 3995-4002.

16. Liu Y, Bartlett JA, Di ME, Bomberger JM, Chan YR, Gakhar L *et al.* SPLUNC1/BPIFA1 contributes to pulmonary host defense against Klebsiella pneumoniae respiratory infection. *Am J Pathol* 2013; **182**(5)**:** 1519-1531.

17. Thaikoottathil JV, Martin RJ, Di PY, Minor M, Case S, Zhang B *et al.* SPLUNC1 deficiency enhances airway eosinophilic inflammation in mice. *Am J Respir Cell Mol Biol* 2012; **47**(2)**:** 253-260.

18. Leeming GH, Kipar A, Hughes DJ, Bingle L, Bennett E, Moyo NA *et al.* Gammaherpesvirus infection modulates the temporal and spatial expression of SCGB1A1 (CCSP) and BPIFA1 (SPLUNC1) in the respiratory tract. *Lab Invest* 2015; **95**(6)**:** 610-624.

19. World Health Organization. Influenza (seasonal) fact sheet. http://www.who.int/mediacentre/factsheets/fs211/en/, 2014, Accessed Date Accessed 2014 Accessed.

20. Wright PF, Neumann G, Kawaoka Y. Orthomyxoviruses. In: Knipe DM, Howley PM (eds). *Fields Virology*, vol. 2. Lippincott, Williams and Wilkins: Philadelphia, 2007, pp 1691-1741.

21. Krammer F, Palese P. Advances in the development of influenza virus vaccines. *Nat Rev Drug Discov* 2015; **14**(3)**:** 167-182.

22. Zaraket H, Saito R, Suzuki Y, Baranovich T, Dapat C, Caperig-Dapat I *et al.* Genetic makeup of amantadine-resistant and oseltamivir-resistant human influenza A/H1N1 viruses. *J Clin Microbiol* 2010; **48**(4)**:** 1085-1092.

23. Portela A, Digard P. The influenza virus nucleoprotein: a multifunctional RNA-binding protein pivotal to virus replication. *J Gen Virol* 2002; **83**(Pt 4)**:** 723-734.

24. Skehel JJ, Wiley DC. Receptor binding and membrane fusion in virus entry: the influenza hemagglutinin. *Annu Rev Biochem* 2000; **69:** 531-569.

25. Wharton SA, Belshe RB, Skehel JJ, Hay AJ. Role of virion M2 protein in influenza virus uncoating: specific reduction in the rate of membrane fusion between virus and liposomes by amantadine. *J Gen Virol* 1994; **75 ( Pt 4):** 945-948.

26. Boulo S, Akarsu H, Ruigrok RW, Baudin F. Nuclear traffic of influenza virus proteins and ribonucleoprotein complexes. *Virus Res* 2007; **124**(1-2)**:** 12-21.

27. Huang L, Li L, Klonowski KD, Tompkins SM, Tripp RA, Mellor AL. Induction and role of indoleamine 2,3 dioxygenase in mouse models of influenza a virus infection. *PLoS One* 2013; **8**(6)**:** e66546.

28. You Y, Richer EJ, Huang T, Brody SL. Growth and differentiation of mouse tracheal epithelial cells: selection of a proliferative population. *Am J Physiol Lung Cell Mol Physiol* 2002; **283**(6)**:** L1315-1321.

29. You Y, Brody SL. Culture and differentiation of mouse tracheal epithelial cells. *Methods Mol Biol* 2013; **945:** 123-143.

30. Leclair EE. Four BPI (bactericidal/permeability-increasing protein)-like genes expressed in the mouse nasal, oral, airway and digestive epithelia. *Biochem Soc Trans* 2003; **31**(Pt 4)**:** 801-805.

31. Bingle L, Cross SS, High AS, Wallace WA, Devine DA, Havard S *et al.* SPLUNC1 (PLUNC) is expressed in glandular tissues of the respiratory tract and in lung tumours with a glandular phenotype. *J Pathol* 2005; **205**(4)**:** 491-497.

32. Bouvier NM, Lowen AC. Animal Models for Influenza Virus Pathogenesis and Transmission. *Viruses* 2010; **2**(8)**:** 1530-1563.

33. Meng B, Marriott AC, Dimmock NJ. The receptor preference of influenza viruses. *Influenza Other Respir Viruses* 2010; **4**(3)**:** 147-153.

34. Kesimer M, Ehre C, Burns KA, Davis CW, Sheehan JK, Pickles RJ. Molecular organization of the mucins and glycocalyx underlying mucus transport over mucosal surfaces of the airways. *Mucosal Immunol* 2013; **6**(2)**:** 379-392.

35. Ehre C, Worthington EN, Liesman RM, Grubb BR, Barbier D, O'Neal WK *et al.* Overexpressing mouse model demonstrates the protective role of Muc5ac in the lungs. *Proc Natl Acad Sci U S A* 2012; **109**(41)**:** 16528-16533.

36. Radicioni G, Cao R, Carpenter J, Ford AA, Wang TT, Li Y *et al.* The innate immune properties of airway mucosal surfaces are regulated by dynamic interactions between mucins and interacting proteins: the mucin interactome. *Mucosal Immunol* 2016; **doi: 10.1038/mi.2016.27. [Epub ahead of print]**.

37. Ghafouri B, Irander K, Lindbom J, Tagesson C, Lindahl M. Comparative proteomics of nasal fluid in seasonal allergic rhinitis. *J Proteome Res* 2006; **5**(2)**:** 330-338.

38. Alva V, Lupas AN. The TULIP superfamily of eukaryotic lipid-binding proteins as a mediator of lipid sensing and transport. *Biochim Biophys Acta* 2016; **1861**(8 Pt B)**:** 913-923.

39. Ning F, Wang C, Berry KZ, Kandasamy P, Liu H, Murphy RC *et al.* Structural characterization of the pulmonary innate immune protein SPLUNC1 and identification of lipid ligands. *FASEB J* 2014; **28**(12)**:** 5349-5360.

40. Britto CJ, Liu Q, Curran DR, Patham B, Dela Cruz CS, Cohn L. Short palate, lung, and nasal epithelial clone-1 is a tightly regulated airway sensor in innate and adaptive immunity. *Am J Respir Cell Mol Biol* 2013; **48**(6)**:** 717-724.

41. Chu HW, Gally F, Thaikoottathil J, Janssen-Heininger YM, Wu Q, Zhang G *et al.* SPLUNC1 regulation in airway epithelial cells: role of Toll-like receptor 2 signaling. *Respir Res* 2010; **11:** 155.

42. Zhou HD, Li XL, Li GY, Zhou M, Liu HY, Yang YX *et al.* Effect of SPLUNC1 protein on the Pseudomonas aeruginosa and Epstein-Barr virus. *Mol Cell Biochem* 2008; **309**(1-2)**:** 191-197.

43. Zhang B, Nie X, Xiao B, Xiang J, Shen S, Gong J *et al.* Identification of tissue-specific genes in nasopharyngeal epithelial tissue and differentially expressed genes in nasopharyngeal carcinoma by suppression subtractive hybridization and cDNA microarray. *Genes Chromosomes Cancer* 2003; **38**(1)**:** 80-90.

44. He Y, Zhou G, Zhai Y, Dong X, Lv L, He F *et al.* Association of PLUNC gene polymorphisms with susceptibility to nasopharyngeal carcinoma in a Chinese population. *J Med Genet* 2005; **42**(2)**:** 172-176.

45. Teran LM, Ruggeberg S, Santiago J, Fuentes-Arenas F, Hernandez JL, Montes-Vizuet AR *et al.* Immune response to seasonal influenza A virus infection: a proteomic approach. *Arch Med Res* 2012; **43**(6)**:** 464-469.

46. Matrosovich M, Matrosovich T, Garten W, Klenk HD. New low-viscosity overlay medium for viral plaque assays. *Virol J* 2006; **3:** 63.

47. Stewart JP, Kipar A, Cox H, Payne C, Vasiliou S, Quinn JP. Induction of tachykinin production in airway epithelia in response to viral infection. *PLoS One* 2008; **3**(3)**:** e1673.

48. Kipar A, Kohler K, Leukert W, Reinacher M. A comparison of lymphatic tissues from cats with spontaneous feline infectious peritonitis (FIP), cats with FIP virus infection but no FIP, and cats with no infection. *J Comp Pathol* 2001; **125**(2-3)**:** 182-191.

## Figure Legends

**Figure 1. BPIFA1 protein levels in BAL are modulated after IAV infection.** BAL samples were taken from C57BL/6J mice infected with IAV X-31 at multiple days p.i. The Simple Western (Wes™; ProteinSimple) system was used to quantify BPIFA1 protein using a rabbit anti-mBPIFA1 primary antibody. Equal amounts of protein (120 µg as determined by BCA, Pierce) were loaded per lane. The area of the BPIFA1 peak, in relation to the standard curve, was determined using Compass software (ProteinSimple). Bars represent mean ± SEM ($n$ = 4). Statistically significant differences (One-way ANOVA with Tukey's post-hoc analysis) between groups are represented by square brackets above. * represents p <0.05; ** represents $p < 0.01$.

**Figure 2. BPIFA1 level in airway epithelia is modulated after IAV infection.** Lungs were dissected from C57BL6/J mice that were either mock- or IAV-infected (i.n. with $10^3$ pfu IAV X-31) at multiple days p.i. as indicated. BPIFA1 was detected by IH using rabbit anti-mBPIFA1, visualized with DAB and counter-stained with hematoxylin. The percentage area of epithelium stained (left graph panels) and intensity of staining (right graph panels) in the trachea (**A**), bronchi (**B**) and bronchioles (**C**) were assessed by image analysis. Data are for four mice per group presented as mean ± SEM. Statistically significant differences (One-way ANOVA with Tukey's post-hoc analysis) between groups are represented by square brackets above. * represents p <0.05, ** represents $p < 0.01$, *** represents $p < 0.001$. Micrographs of representative areas at each time point are shown below the graph panels. Black arrows point to expression of BPIFA1 in respiratory epithelium. Scale bars represent; panel A: 50 µm, panel B: 10 µm and panel C:20 µm.

**Figure 3. BPIFA1 influences the infection of mice by IAV. Panels A, B**. C57BL/6J and *Bpifa1*$^{-/-}$ mice (*n* = 4 per group) were infected i.n. with $10^3$ pfu IAV X-31. **Panel A**. Mice were weighed daily and the weights represented as a percentage of the starting weight. Data represent the mean value ± SEM. Asterisks indicate statistical difference (two-way ANOVA with Bonferroni post-test; **represents $p < 0.01$. **Panel B.** Lung tissues were taken at multiple days p.i. as indicated and virus titer determined by plaque assay. Data represent the mean value ± SEM. Asterisks indicate statistical difference (two-way ANOVA with Bonferroni post-test; * represents $p < 0.05$, *** represents $p < 0.001$). **Panel C**. Bpifa1$^{loxP}$; Scgb1a1-CreER$^{TM}$ mice were treated with either carrier (vegetable oil) or carrier plus Tamoxifen (tmx) by oral gavage five times as described in materials and methods. Lung tissue (*n* = 4 per group) was analyzed by western blotting for BPIFA1. Equal amounts (100 µg) of protein as determined by BCA (Pierce) were loaded per lane. The mean (± SEM) levels of BPIFA1 protein were measured by Image J as integrated band intensity. * represents statistical significance (Mann-Whitney *U* test; $p < 0.05$) BPIFA1 is clearly knocked down in the Tamoxifen-treated animals. **Panel D**. Tamoxifen-inducible, club cell specific BPIFA1 knockout mice (*Bpifa1*$^{loxP}$; *Scgb1a1-CreER*$^{TM}$) were dosed on 5 consecutive days by gavage with 0.25 mg per gram body weight tamoxifen (tmx) or carrier (vegetable oil). Four days after the last gavage these mice, along with untreated *Bpifa1*$^{loxP}$; *Scgb1a1-CreER*$^{TM}$ and *Bpifa1*$^{-/-}$ mice (*n* = 4 for all groups) were infected with IAV for 7 days. Lungs were collected and virus titer determined by plaque assay. Data represent the mean value ± SEM. Asterisks indicate statistical difference (One-way ANOVA with Tukey's post-hoc analysis; $p < 0.05$).

**Figure 4. IAV spreads more rapidly in the absence of BPIFA1.** C57BL/6J and *Bpifa1*$^{-/-}$ mice were infected i.n. with $10^3$ pfu IAV X-31. Lung tissues were harvested at one day p.i. IAV antigen was detected by IH using goat anti-IAV, visualized with DAB and counter-stained with hematoxylin. Micrographs of representative areas from distal bronchioles and alveoli four mice are shown. Large arrows, positive epithelial cells. Red arrowheads, positive macrophages.

**Figure 5. BPIFA1 influences the infection of normal mTEC by IAV.** mTEC ALI cultures were infected with IAV X-31 (0.1 pfu/cell). Panels **A – F**. Cells were processed and stained with anti-IAV NP (green), anti-mBPIFA1 (red), nuclei counterstained with DAPI (blue) and imaged using a confocal microscope. Scale bar represents 50 µm. Micrographs show representative areas from C57BL/6J mTEC cultures **(A, B, C)** and *Bpifa1*$^{-/-}$ mTEC cultures **(D, E, F)** at 2, 24 and 48 h p.i. **(G)** Mean integrated florescence intensity IAV nucleoprotein in mTEC ALI shown for 3 independent biological replicates (± SEM). * represents $p < 0.05$, One-way ANOVA with Tukey's post-hoc analysis. **(H)** Titer of IAV in apical wash. Data presented as mean ± SEM; n = 3; * represents $p < 0.05$, One-way ANOVA with Tukey's post-hoc analysis.

**Figure 6. BPIFA1 decreases the nuclear import of IAV RNPs into normal mTEC.** mTEC ALI cultures from *wt* C57BL/6J or *Bpifa1*$^{-/-}$ mice were incubated with purified IAV A/PR/8/34 in the presence or absence of cycloheximide (CHX) as indicated. Cycloheximide blocks protein synthesis and so indicates the import of pre-existing IAV RNP from incoming virus particles. After 4 h incubation at 37°C cultures were processed and stained with anti-IAV NP and counter-stained with DAPI before

visualization using a confocal microscope. Scale bar represents 50 μm. (**A**) Representative micrographs from cultures incubated with IAV in the absence or presence of CHX (**B**) micrographs from cultures incubated with IAV in presence of CHX at a higher magnification. (**C**) Nuclei that were positive for IAV NP in the presence of cycloheximide were counted at 40x magnification in five fields (one center and four peripheral fields) per sample and presented as a percentage of positive cells over total cells counted. The mean percentage positive nuclei are shown for 3 independent biological replicates (± SEM). * represents statistical significance (One-way ANOVA with Tukey's post-hoc analysis; $p < 0.05$)

**Figure 7. BPIFA1 restricts binding of IAV to normal epithelial cells in mTEC ALI cultures.** mTEC ALI cultures were incubated for 1 h with IAV Alexa-fluor 488-labeled purified IAV A/PR/8/34 (IAV-488), then fixed with formalin, stained with anti-BPIFA1 and anti-FoxJ1 antibodies and then imaged using a confocal microscope (**A**) Representative images of two different fields of day 14 C57BL/6J mTEC ALI culture showing IAV-488 (green) preferentially binding to FoxJ1-positive (white) ciliated cells but not BPIFA1 (red)-positive cell populations (circled by yellow dotted line). (**B**) Micrograph showing IAV-488 binding (green) with the epithelium of *wt* C57BL/6 and *Bpifa1*$^{-/-}$ cultures. (**C**) Integrated florescence intensity of IAV-488 virus binding with the surfaces of mTEC culture. Images were captured from at least five fields per sample by confocal microscope at 20x, 40x and 60x magnification. The levels of IAV-488 binding on mTEC cell surfaces were measured by Image J as integrated fluorescence intensity. The mean fluorescent intensity is shown for 3 independent biological replicates (± SEM). * represents statistical significance (Mann-Whitney *U* test; $p < 0.05$)

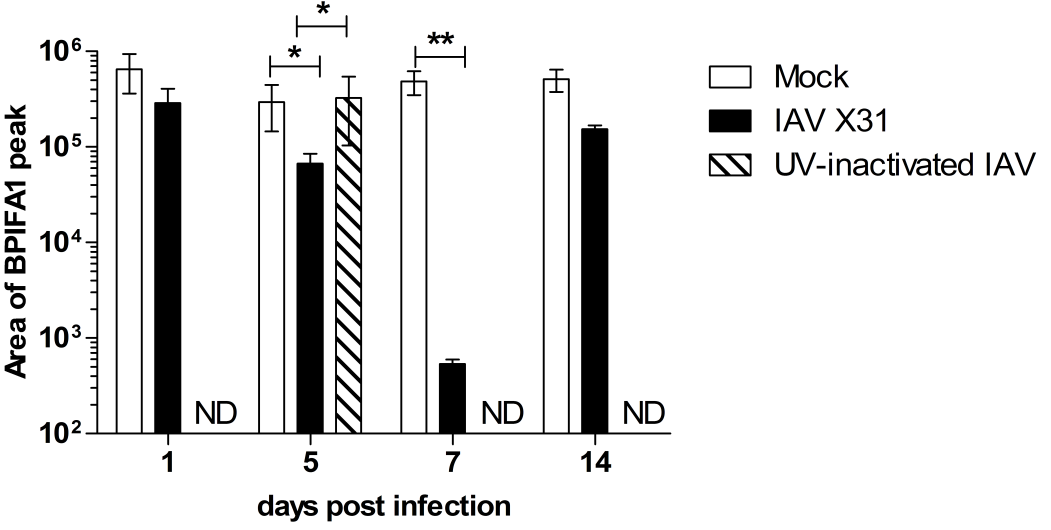
Area of BPIFA1 peak
$10^6$
$10^5$
$10^4$
$10^3$
$10^2$
ND
ND
ND
1
5
7
14
days post infection
*
*
**
Mock
IAV X31
UV-inactivated IAV

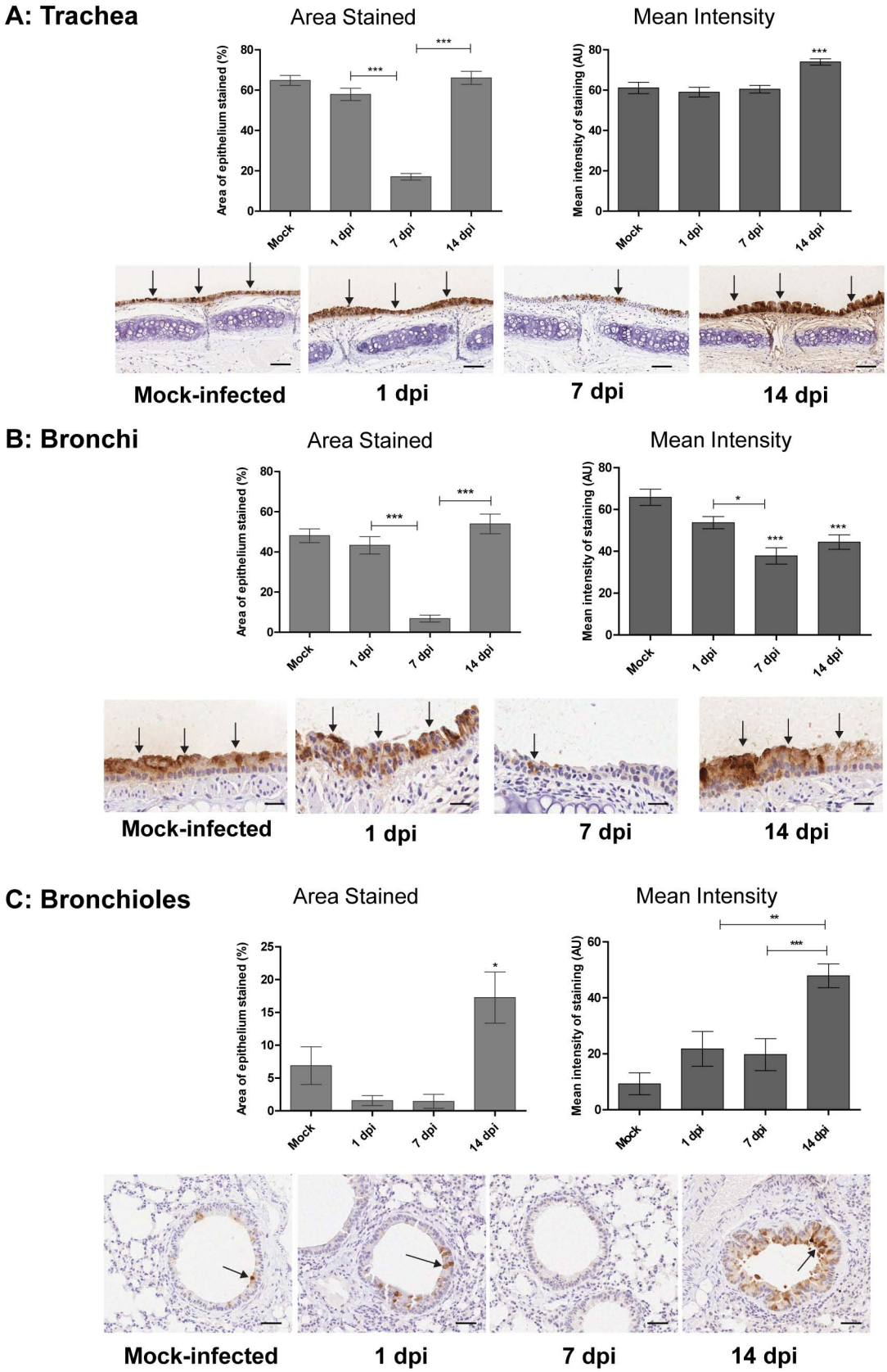
A: Trachea
Area Stained
Mean Intensity
Area of epithelium stained (%)
Mean intensity of staining (AU)
Mock
1 dpi
7 dpi
14 dpi
Mock-infected
1 dpi
7 dpi
14 dpi
B: Bronchi
Area Stained
Mean Intensity
Area of epithelium stained (%)
Mean intensity of staining (AU)
Mock
1 dpi
7 dpi
14 dpi
Mock-infected
1 dpi
7 dpi
14 dpi
C: Bronchioles
Area Stained
Mean Intensity
Area of epithelium stained (%)
Mean intensity of staining (AU)
Mock
1 dpi
7 dpi
14 dpi
Mock-infected
1 dpi
7 dpi
14 dpi

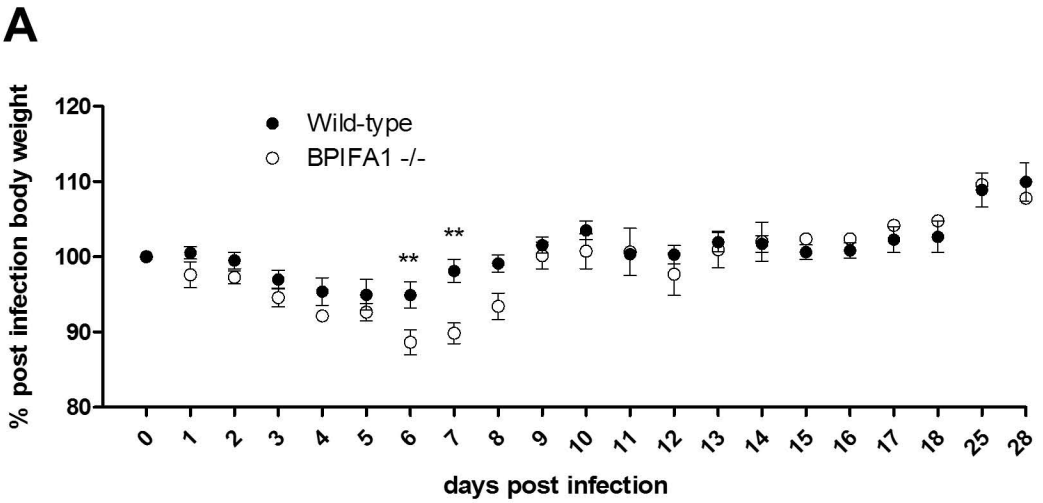
A
% post infection body weight
120
110
100
90
80
Wild-type
BPIFA1 -/-
**
**
0 1 2 3 4 5 6 7 8 9 10 11 12 13 14 15 16 17 18 25 28
days post infection

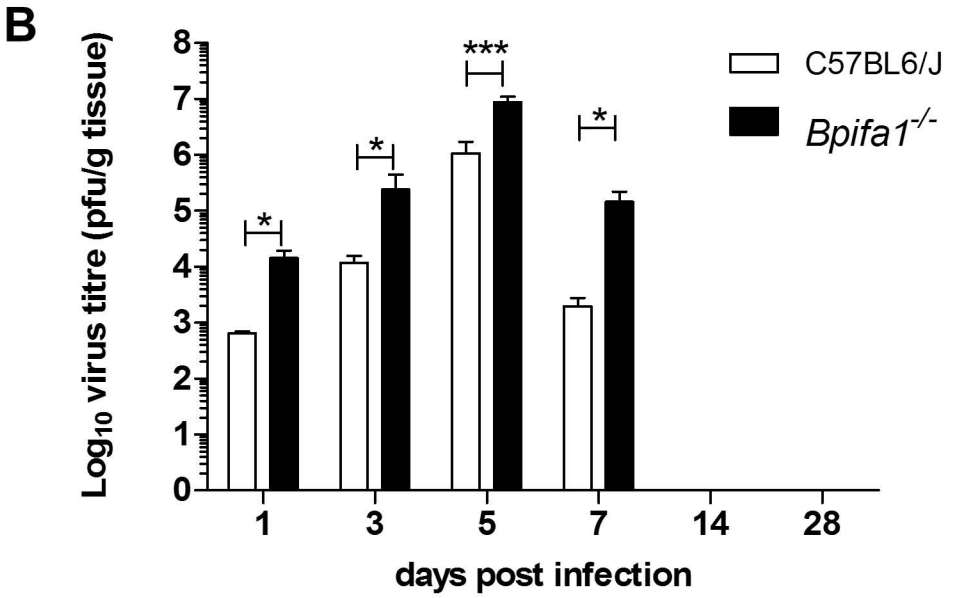
B
Log10 virus titre (pfu/g tissue)
8
7
6
5
4
3
2
1
0
*
*
***
*
C57BL6/J
Bpifa1-/-
1 3 5 7 14 28
days post infection

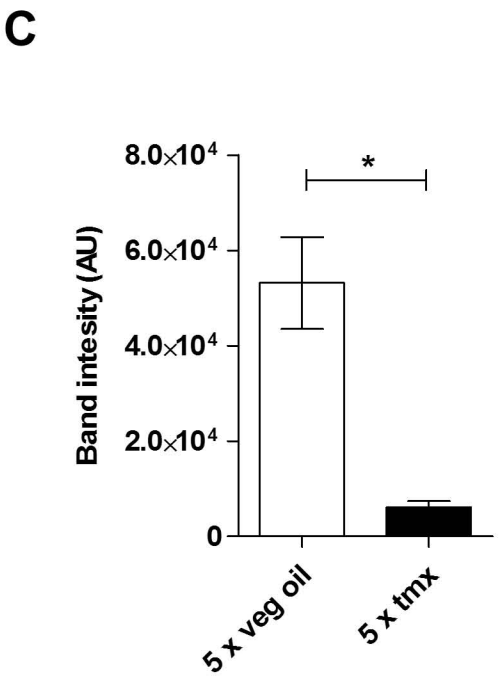
C
Band intesity (AU)
8.0×10^4
6.0×10^4
4.0×10^4
2.0×10^4
0
*
5 x veg oil
5 x tmx

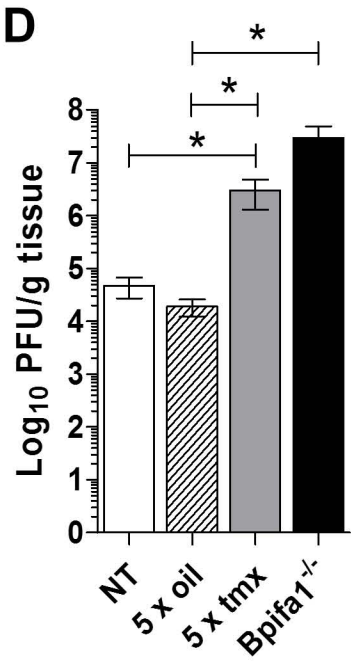
D
Log10 PFU/g tissue
8
7
6
5
4
3
2
1
0
*
*
*
NT
5 x oil
5 x tmx
Bpifa1-/-

Distal bronchioles

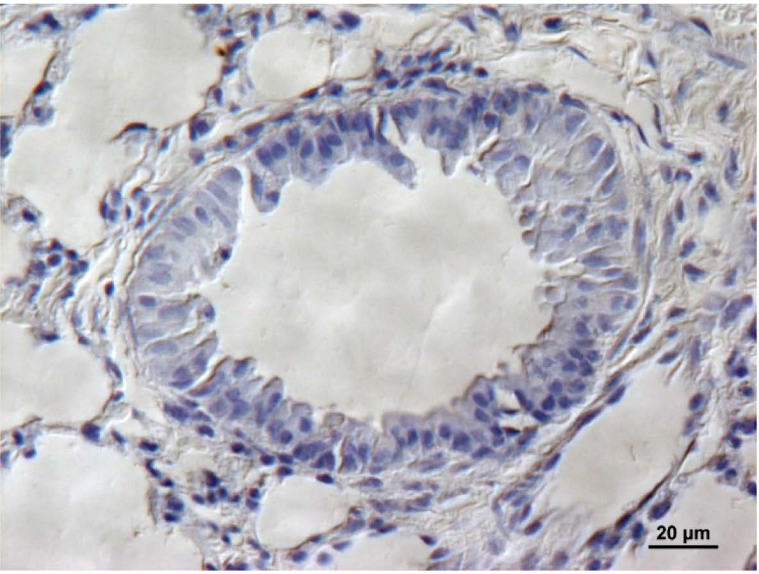


*wt*

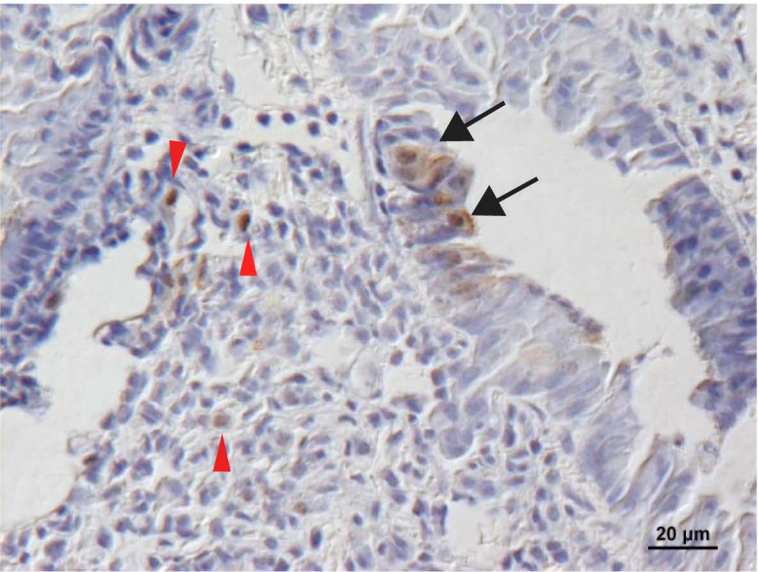


*Bpifa1* $^{-/-}$

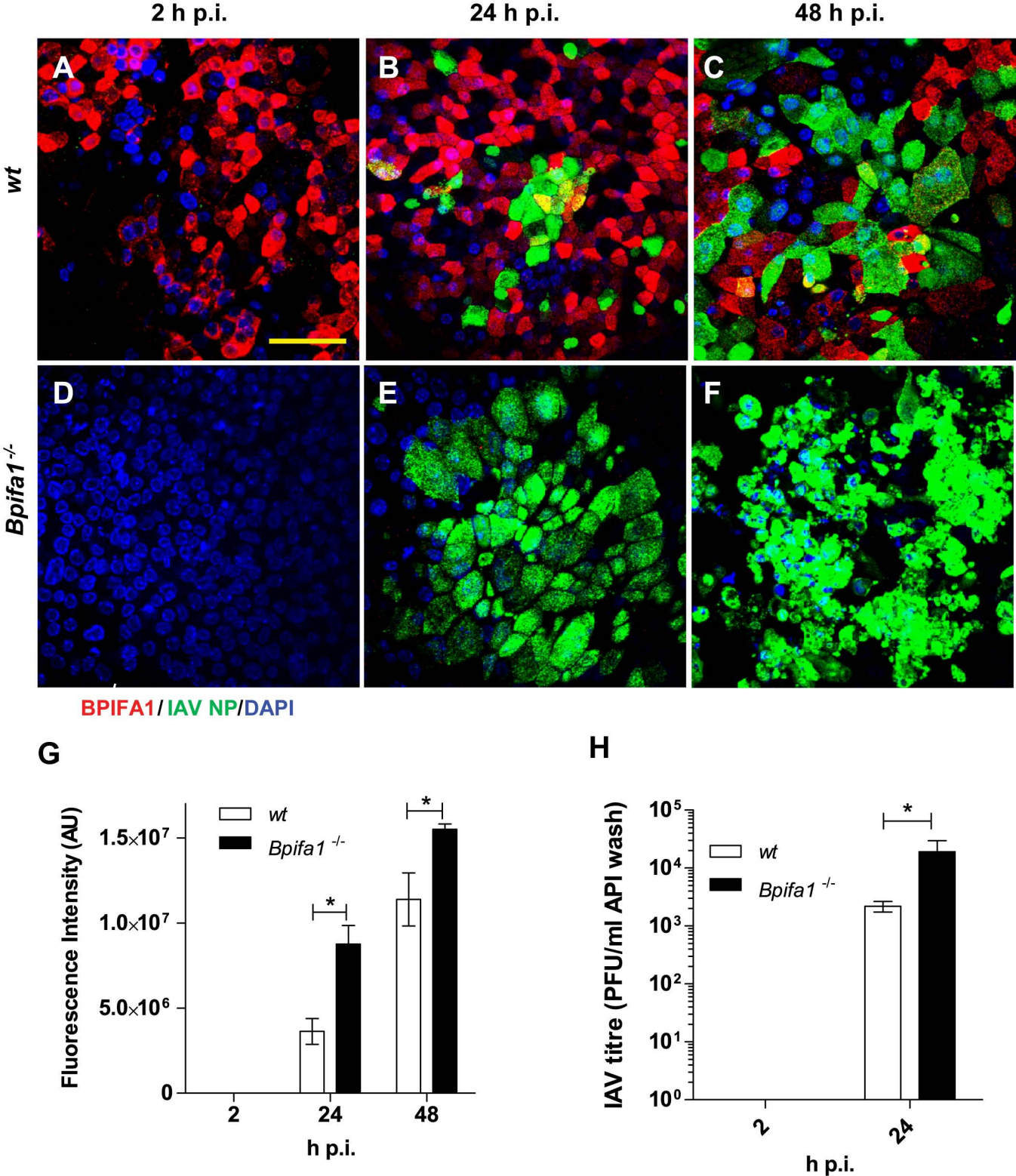
2 h p.i.
24 h p.i.
48 h p.i.
wt
Bpifa1 -/-
A
B
C
D
E
F
BPIFA1 / IAV NP / DAPI
G
Fluorescence Intensity (AU)
1.5×10^7
1.0×10^7
5.0×10^6
0
wt
Bpifa1 -/-
*
*
2
24
48
h p.i.
H
IAV titre (PFU/ml API wash)
10^5
10^4
10^3
10^2
10^1
10^0
wt
Bpifa1 -/-
*
2
24
h p.i.

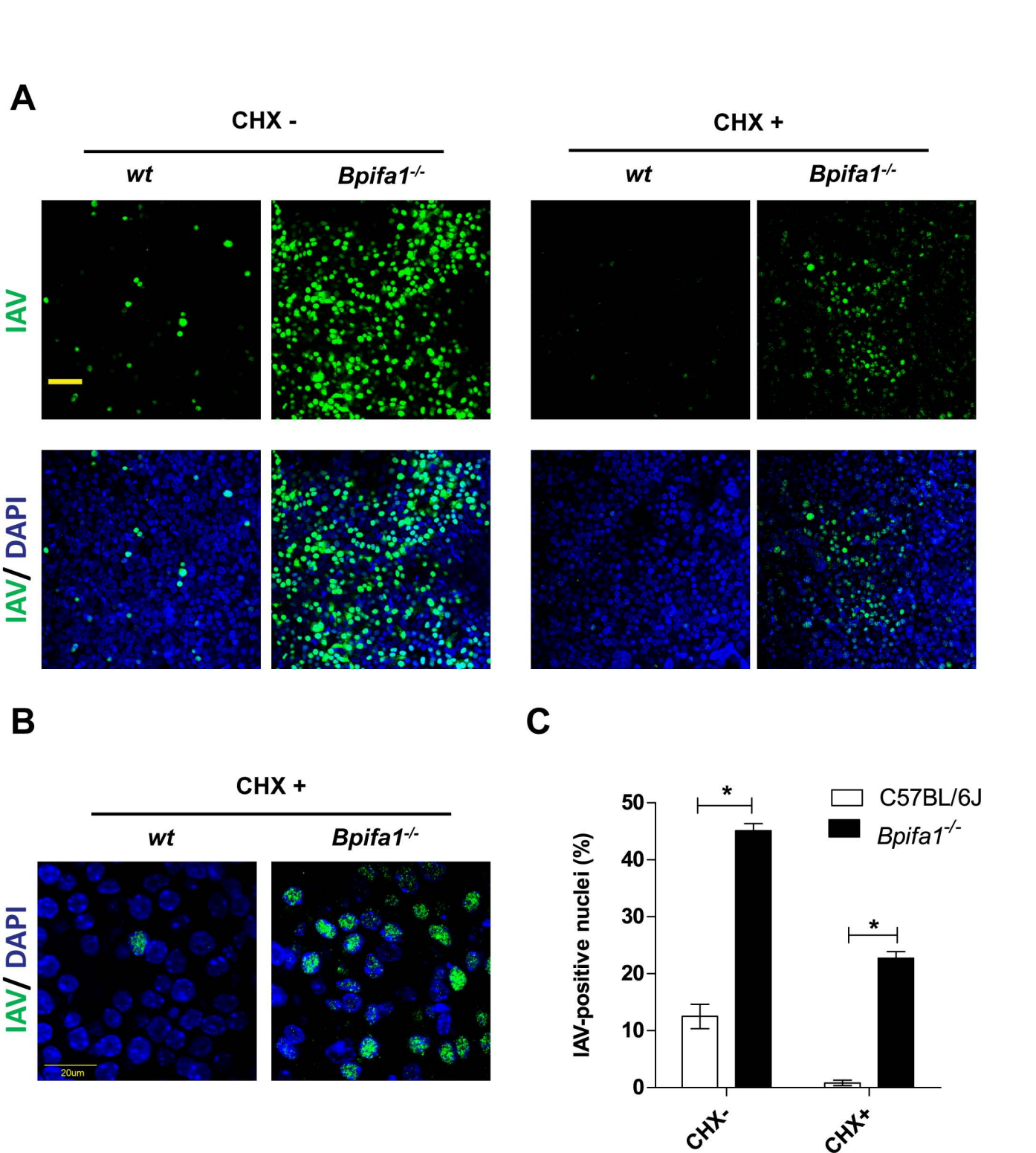
A
CHX -
CHX +
wt
Bpifa1-/-
wt
Bpifa1-/-
IAV
IAV/ DAPI
B
CHX +
wt
Bpifa1-/-
IAV/ DAPI
20um
C
IAV-positive nuclei (%)
50
40
30
20
10
0
*
*
C57BL/6J
Bpifa1-/-
CHX-
CHX+

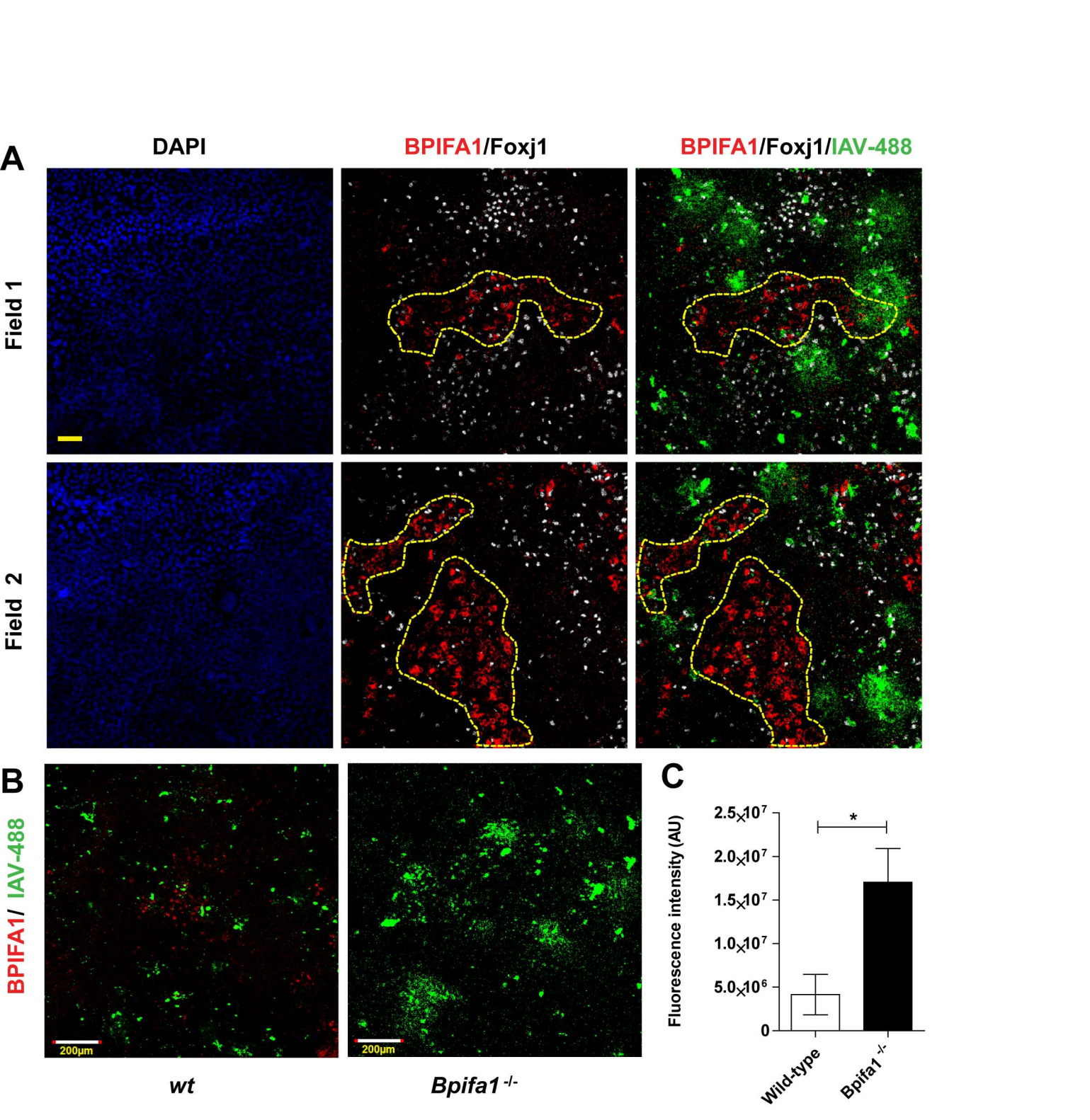
A
DAPI
BPIFA1/Foxj1
BPIFA1/Foxj1/IAV-488
Field 1
Field 2
B
BPIFA1/ IAV-488
200µm
200µm
wt
Bpifa1 -/-
C
Fluorescence intensity (AU)
2.5x10^7
2.0x10^7
1.5x10^7
1.0x10^7
5.0x10^6
0
*
Wild-type
Bpifa1 -/-

**Supplementary Data**

## Results

### Generation of transgenic mice deficient in BPIFA1.

Animal procedures for generation of the *Bpifa1*$^{loxP}$ and *Bpifa1*$^{-/-}$ transgenic lines were approved by the Institutional Animal Care and Use Committee at University of Hawaii under protocols 07-056 and 11-1112.

A conditional targeting vector for *Bpifa1* used for transfection of C57BL/6J mouse embryonic stem cells was constructed by InGenious Targeting Laboratory, Inc. (Ronkonkoma, NY). The targeted region on the *Bpifa1* gene includes exons 2-3 (see S1 Fig. A).

Embryonic stem cells were microinjected into BALB/c blastocysts. Resulting chimeras with a high percentage black coat color were mated to wild-type C57BL/6J mice to generate F1 heterozygous offspring. Correctly targeted F1 mice contained a Neo-selection cassette, three lox-P sites and two FRT sites.

Deletion of the Neo-cassette was achieved by breeding with a heterozygous C57BL/6J background FLP$^{+/-}$ mouse (Jackson Laboratories, JAX; stock# 003800). Since these FLP mice are heterozygotes (homozygotes are embryonic lethal), the resulting F2 mosaic mice were screened for presence of the FLP transgene and deletion of the Neo cassette. After breeding with C56BL/6J mice, the resulting F3 generation was screened for FLP transgene absence and deletion of the Neo cassette. This mouse was bred with another heterozygous FLP$^{-/-}$ and Neo$^{-/-}$ F3 offspring to produce a homozygous floxed F4 mouse without the FLP transgene and without the Neo cassette (*Bpifa1*$^{loxP}$).

To generate a systemic *Bpifa1* KO mouse *(Bpifa1*$^{-/-}$), *Bpifa1*$^{loxP}$ mice were mated with a mouse containing the Cre-recombinase transgene under the control of

hCMV IE promoter (CMV-Cre, formally B6.C-Tg(Tg (CMV-Cre)1Cgn/J; JAX Stock No: 006054; see S1 Fig. A).

*Bpifa1*$^{loxP}$ and *Bpifa1*$^{-/-}$ mice were deposited at the MRC Mammalian Genetics Unit (Harwell, UK; FESA:5217 and 5945 respectively) and then transferred from there to the University of Liverpool.

To generate a conditional, club cell-specific KO mouse (*Bpifa1*$^{loxP}$; *Scgb1a1-CreER*$^{TM}$), *Bpifa1*$^{loxP}$ mice were mated with *Scgb1a1-CreER*$^{TM}$ (*Scgb1a1*$^{tm1(cre/ERT)Blh}$; Jackson Lab, stock# 016225) [1]. These mice express a tamoxifen-inducible form of cre recombinase from the *Scgb1a1* locus (secretoglobin).

**Phenotyping of *Bpifa1*$^{-/-}$ mice.**

Four wild type (*wt*) mice (C57BL/6J) and four *Bpifa1*$^{-/-}$ mice, two males and two females of each, aged 6 – 10 weeks, were examined grossly and histologically for phenotypical differences as a result of lack of expression of the *Bpifa1* gene. There were no differences grossly. Histological examination of the lymphoid, gastrointestinal, urinary, cardiovascular, endocrine, reproductive organs and the CNS was unremarkable. In addition to the respiratory tract, BPIFA1 is expressed in minor glands of the nose, sinuses, posterior tongue and tonsil [2, 3], in some of the seromucous cells of the major salivary glands and is detectable in saliva. In glandular tissues examined (submandibular, parotid and sub-lingual salivary glands, minor tongue (von Ebner's) gland, Zymbal's gland, Harderian gland and lacrimal gland), the only difference noted was that the eosinophilic granules within the epithelium of the convoluted tubules of the submandibular salivary glands, which are prominent in male mice only, were far less striking in the male *Bpifa1*$^{-/-}$ mice. The serous and mucous

glands were unaffected, and Alcian blue (AB) and periodic acid-Schiff (PAS) staining yielded similar results in both *wt* and *Bpifa1*$^{-/-}$ mice in these glands (data not shown).

The tissues of the upper and lower respiratory tract were examined using H&E, AB and PAS stains, as well as immunohistology (IH) for BPIFA1 and SCGB1A1. Tissues from *Bpifa1*$^{-/-}$ were consistently IH-negative for BPIFA1, and there were no differences in the intensity or distribution of SCGB1A1 immunostaining between the *wt* and the *Bpifa1*$^{-/-}$ mice. In *Bpifa1*$^{-/-}$ mice the nasal respiratory epithelial cells at the transition to the olfactory epithelium generally exhibited abundant hyalinized globular cytoplasmic material, leading to expansion of the cells (S1 Fig C). This is a common finding in many strains of mice and increases in severity with age [4-6] but is of interest as in the present study it was only present in the *Bpifa1*$^{-/-}$ mice, and at this young age. In the trachea, bronchi and lower respiratory tract, no phenotypical differences were noted between the wild type and *Bpifa1*$^{-/-}$ mice.

**Normal tracheal epithelial cultures (mTEC) are a good model to study IAV infection in vitro.**

Normal mouse tracheal cell cultures were established from C57BL/6J mice and cultured at the air-liquid interface to generate well-differentiated cultures (mTEC). Differentiated mTEC ALI cultures displayed phenotypic features associated with a complex population of ciliated cells (β-tubulin), BPIFA1, mucin (MUC5B), Foxj1 (cilia marker) and SCGB1A1 (CCSP)-expressing cells that matched with the features of the native rodent airway epithelium (S3 Fig. A, C, D, E). The surface topology of day 14-differentiated mTEC ALI cultures also showed ciliated epithelial cells interspersed with domed shaped non-ciliated cells with a cobble stone appearance, which is typical of the upper airway morphology (S3 Fig. B). The expression of a selected cohort of

airway epithelium-specific genes was also assessed in 14-day cultures to further validate our *in vitro* model. SCGB1A1 (a club cell marker), and BPIFB1 (LPLUNC1) gene expression was present but relatively low when compared with mTEC original cells (freshly isolated mTEC cells without culture modification) (S3 Fig. F). BPIFA1 was readily detected in cultured epithelial cells and within the apical secretions (S3 Fig. A, G) but was not found in ciliated cells (S3 Fig. A, C). Airway epithelium-associated genes, *Bpifa1*, *Bpifb1, Scgb1a1, Muc5ac*, *Muc5b*, *Tekt-1* (a cilia gene) were consistently expressed in Day-14 mTEC ALI cultures and matched with the original cell gene expression signature of the mTECs (S3 Fig. F). The *in vitro* tracheal cultures are thus a good *in vitro* model with which to study BPIFA1 biology during IAV infection.

## References


1. Rawlins EL, Okubo T, Xue Y, Brass DM, Auten RL, Hasegawa H, et al. The role of Scgb1a1+ Clara cells in the long-term maintenance and repair of lung airway, but not alveolar, epithelium. Cell stem cell. 2009;4(6):525-34. doi: 10.1016/j.stem.2009.04.002. PubMed PMID: 19497281; PubMed Central PMCID: PMC2730729.

2. Bingle L, Cross SS, High AS, Wallace WA, Devine DA, Havard S, et al. SPLUNC1 (PLUNC) is expressed in glandular tissues of the respiratory tract and in lung tumours with a glandular phenotype. J Pathol. 2005;205(4):491-7. Epub 2005/02/03. doi: 10.1002/path.1726. PubMed PMID: 15685591.

3. Musa M, Wilson K, Sun L, Mulay A, Bingle L, Marriott HM, et al. Differential localisation of BPIFA1 (SPLUNC1) and BPIFB1 (LPLUNC1) in the nasal and oral cavities of mice. Cell Tissue Res. 2012;350(3):455-64. Epub 2012/09/19. doi:

10.1007/s00441-012-1490-9. PubMed PMID: 22986921; PubMed Central PMCID: PMC3505551.

4. Taylor I. Chapter 4 - Mouse In: McInnes EF, editor. Background Lesions in Laboratory Animals. Saint Louis: W.B. Saunders; 2012. p. 45-72.

5. Ward JM, Yoon M, Anver MR, Haines DC, Kudo G, Gonzalez FJ, et al. Hyalinosis and Ym1/Ym2 gene expression in the stomach and respiratory tract of 129S4/SvJae and wild-type and CYP1A2-null B6, 129 mice. Am J Pathol. 2001;158(1):323-32. doi: 10.1016/S0002-9440(10)63972-7. PubMed PMID: 11141507; PubMed Central PMCID: PMCPMC1850245.

6. Renne R, Brix A, Harkema J, Herbert R, Kittel B, Lewis D, et al. Proliferative and nonproliferative lesions of the rat and mouse respiratory tract. Toxicologic pathology. 2009;37(7 Suppl):5S-73S. Epub 2010/02/06. doi: 10.1177/0192623309353423. PubMed PMID: 20032296.

7. de Jonge HJ, Fehrmann RS, de Bont ES, Hofstra RM, Gerbens F, Kamps WA, et al. Evidence based selection of housekeeping genes. PLoS One. 2007;2(9):e898. doi: 10.1371/journal.pone.0000898. PubMed PMID: 17878933; PubMed Central PMCID: PMCPMC1976390.

## Supplementary Figure Legends

**S1 Fig. Construction and characterisation of *Bpifa1*$^{loxP}$ and *Bpifa1*$^{-/-}$ mice**

**Panel A (i).** Wild-type *Bpifa1* locus. The targeted region on the *Bpifa1* gene includes exons 2-3. **(ii).** Targeting vector. The conditional targeting vector contained exons 2 and 3 flanked by LoxP sites and a Neo selection cassette flanked by FRT sites. **(iii).** Deletion of the Neo-cassette was achieved by breeding with a heterozygous C57BL/6J background FLP$^{+/-}$ mouse to generate conditional targeted *Bpifa1*$^{loxP}$ mice. **(iv)**. To generate a systemic *Bpifa1* KO mouse *(Bpifa1*$^{-/-}$), *Bpifa1*$^{loxP}$ mice were mated with a

mouse containing the Cre-recombinase transgene under the control of hCMV IE promoter.

**Panel B.** Western blot analysis of lung tissue from either wild-type C57BL/6J or *Bpifa1*$^{-/-}$ mice (as indicated) using rabbit anti-BPIFA1 as primary antibody. The first lane shows the molecular weight markers. A characteristic 27-31 kDa doublet was observed corresponding to alternatively-glycosylated forms of BPIFA1 in the wild-type but not *Bpifa1*$^{-/-}$ mice.

**Panel C.** Nasal cavities of C57BL/6J and *Bpifa1*$^{-/-}$ mice were dissected, processed for histology and stained with hematoxylin/eosin. In *Bpifa1*$^{-/-}$ mice there was hyalinised globular cytoplasmic material present in the respiratory epithelium at the transition to olfactory epithelium shown by black arrows. Micrographs of representative areas from four mice are shown.

**S2 Fig. IAV-specific staining in mice at 1 day p.i.** C57BL/6J and *Bpifa1*$^{-/-}$ mice were infected i.n. with IAV X-31. Lung tissues were taken at one day p.i. IAV antigen was detected by IH using goat anti-IAV, visualized with DAB and counter-stained with hematoxylin. Micrographs of representative areas from four mice are shown. Large arrows, positive epithelial cells.

**S3 Fig. Validation normal tracheal epithelial cell (mTEC) model.** Tracheal epithelial cells were prepared from C57BL/6J mice and differentiated at the air-liquid interface for 14 days. (**A**) Confocal image showing cells stained for β-tubulin (ciliated cells; green) and BPIFA1 (red). The Z-slice (side panels) shows BPIFA1 cells are non-ciliated. (**B**) Scanning electron micrograph of the apical surface of the mTEC cultures showing ciliated cells and non-cilated cells with a cobble-stone appearance. (**C, D, E**)

Confocal images showing BPIFA1 and FoxJ1 (**C**), MUC5B (**D**) and SCGB1A1 (**E**) in day 14 ALI cultures of WT mTECs. (**F**) RT-PCR showing airway epithelium associated gene expression profile of mTEC ALI culture of WT (representative of three independent cultures). The OAZ-1 gene was used as housekeeping gene [7] (**G**) Western blot on apical washes collected from WT mTEC-ALI culture (representative of three independent cultures). Scale bar for confocal images represents 50 μm.

**S4 Fig. Validation of the phenotype of mTEC ALI cultures from *Bpifa1*$^{-/-}$ mice.** mTEC ALI cultures from wild-type C57BL6/J and *Bpifa1*$^{-/-}$ mice were analyzed by confocal microscopy. Micrographs show representative areas from three separate cultrues. Panels **A, B**. Cells were processed and stained with anti-β-tubulin (cilia marker; green), anti-mBPIFA1 (red) and nuclei counterstained with DAPI (blue). Panels **(C, D)** Cells were processed and stained with anti-MUC5B (mucin secreting cells; red) and nuclei counterstained with DAPI (blue). Scale bar represents 50 μm.

**S5 Fig. Detection of α2,3- and α2,6-linked sialic acid residues on uninfected mTEC.** The presence of α2,3-linked sialic acid (SA) and α2,6-linked SA residues on the surface of cells was detected by binding of fluorescein-labelled lectins from *Maackia amurensis* (MAA) and *Sambucus nigra* (SNA), respectively. Uninfected day 14 ALI cultured mTECs were dual-labelled with either anti-BPIFA1 plus MAA or anti-BPIFA1 plus SNA. (**A**) α2,3-linked SA receptor expression (detected by MAA) was present in both *wt* and *Bpifa1*$^{-/-}$ mTEC cultures. Interestingly, the BPIFA1$^{+}$ cell population was absolutely devoid of α2,3-linked SA residue expression. (**B**) α2,6-linked SA receptor expression (detected by SNA) was only seen in a low proportion of

cells in both *wt* and *Bpifa1*$^{-/-}$ mTECs. (**C, D, E**) Occasional expression of α2,6-linked SA residues was detected in BPIFA1$^{+}$ mTECs. This is a representative result from three separate experiments on two batches of mice. Scale bar represents 20 μm.

S1 Fig

**A**

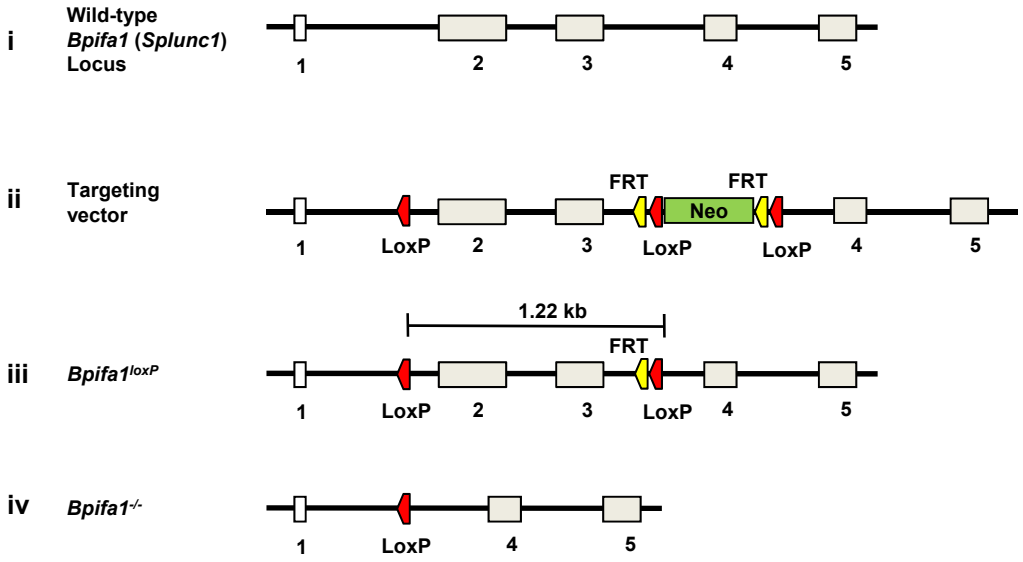
i
Wild-type
Bpifa1 (Splunc1)
Locus
1
2
3
4
5
ii
Targeting
vector
FRT
FRT
Neo
1
LoxP
2
3
LoxP
LoxP
4
5
iii
Bpifa1loxP
1.22 kb
FRT
1
LoxP
2
3
LoxP
4
5
iv
Bpifa1-/-
1
LoxP
4
5

**B**

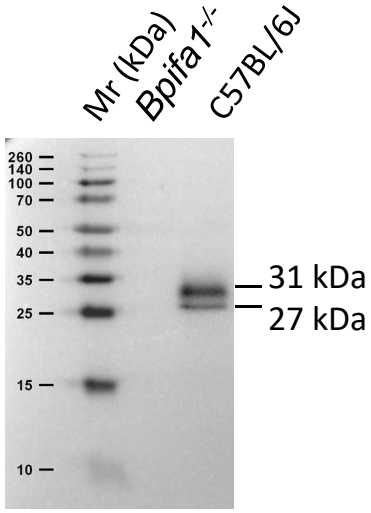
Mr (kDa)
Bpifa1-/-
C57BL/6J
260
140
100
70
50
40
35
25
15
10
31 kDa
27 kDa

**C**

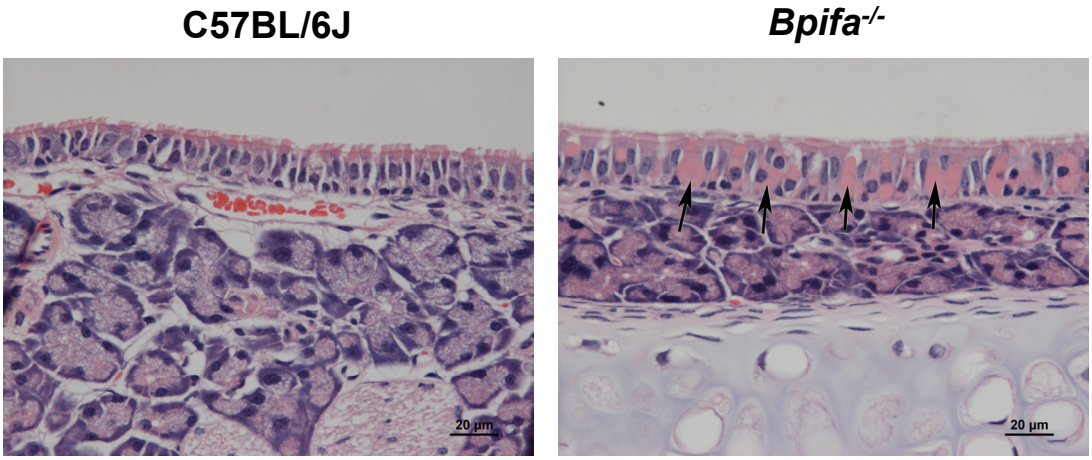
C57BL/6J
Bpifa-/-
20 µm
20 µm

S2 Fig

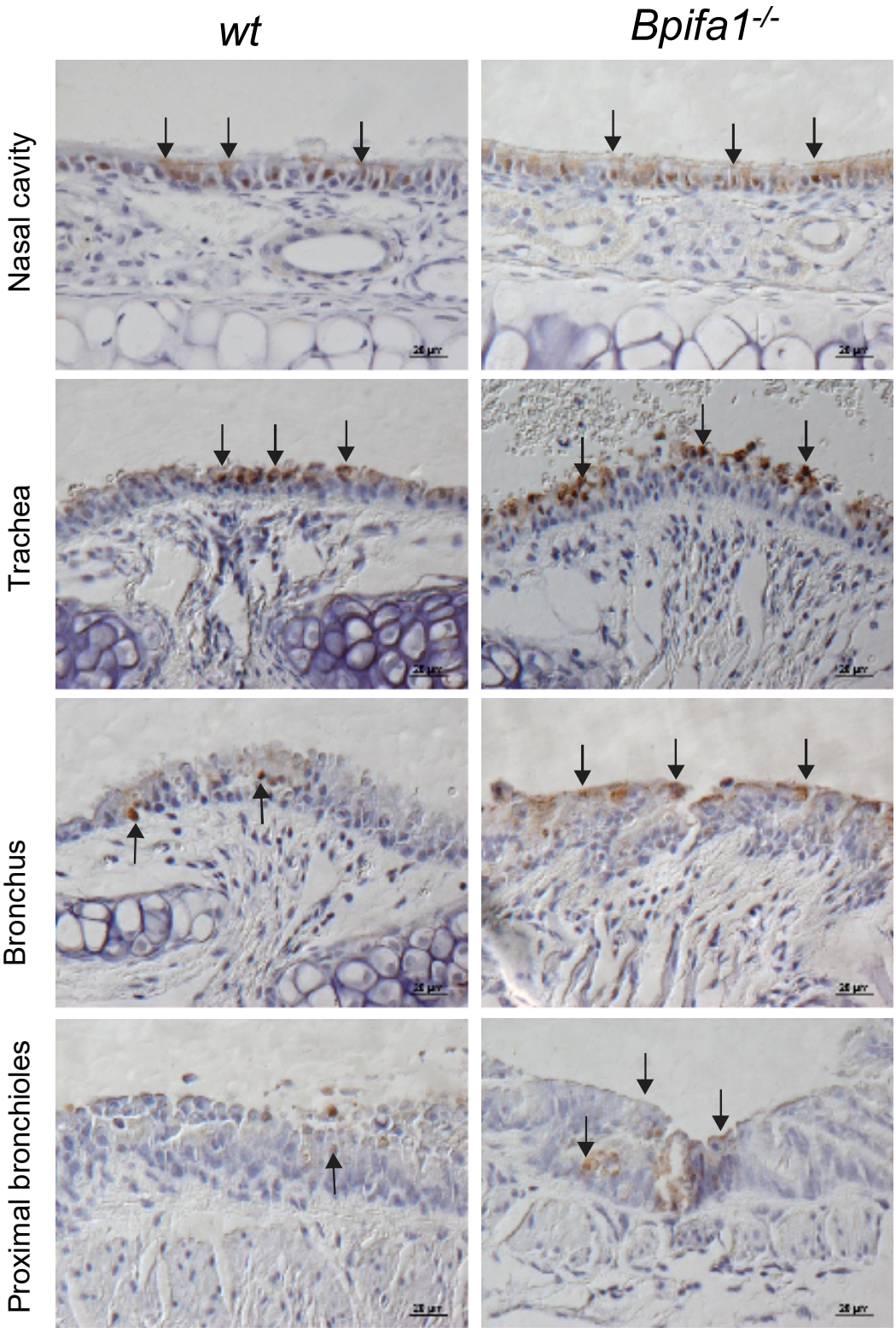
wt
Bpifa1-/-
Nasal cavity
Trachea
Bronchus
Proximal bronchioles

S3 Fig

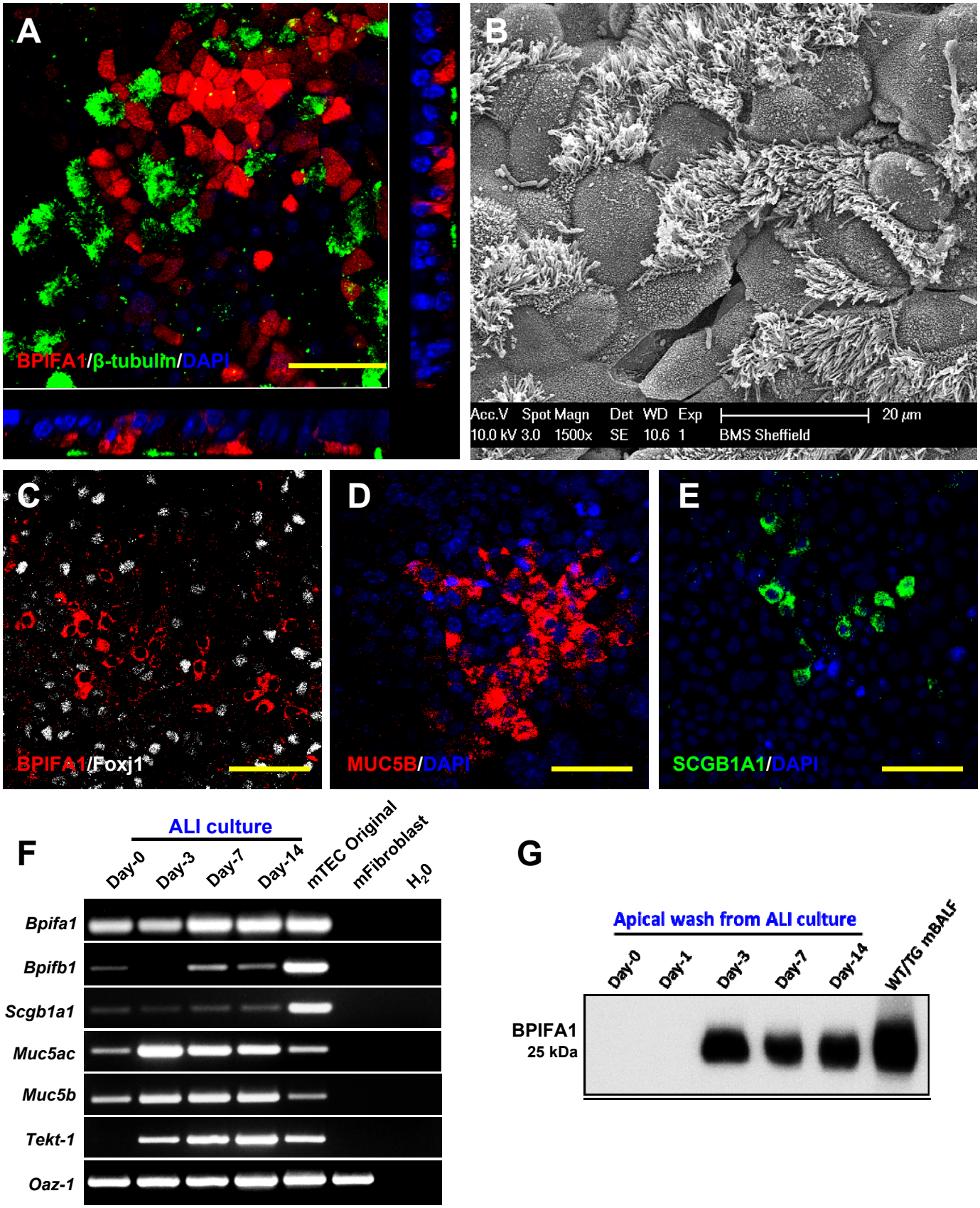
A
BPIFA1/β-tubulin/DAPI
B
Acc.V Spot Magn Det WD Exp 20 μm
10.0 kV 3.0 1500x SE 10.6 1 BMS Sheffield
C
BPIFA1/Foxj1
D
MUC5B/DAPI
E
SCGB1A1/DAPI
F
ALI culture
Day-0
Day-3
Day-7
Day-14
mTEC Original
mFibroblast
H2O
Bpifa1
Bpifb1
Scgb1a1
Muc5ac
Muc5b
Tekt-1
Oaz-1
G
Apical wash from ALI culture
Day-0
Day-1
Day-3
Day-7
Day-14
WT/TG mBALF
BPIFA1
25 kDa

S4 Fig

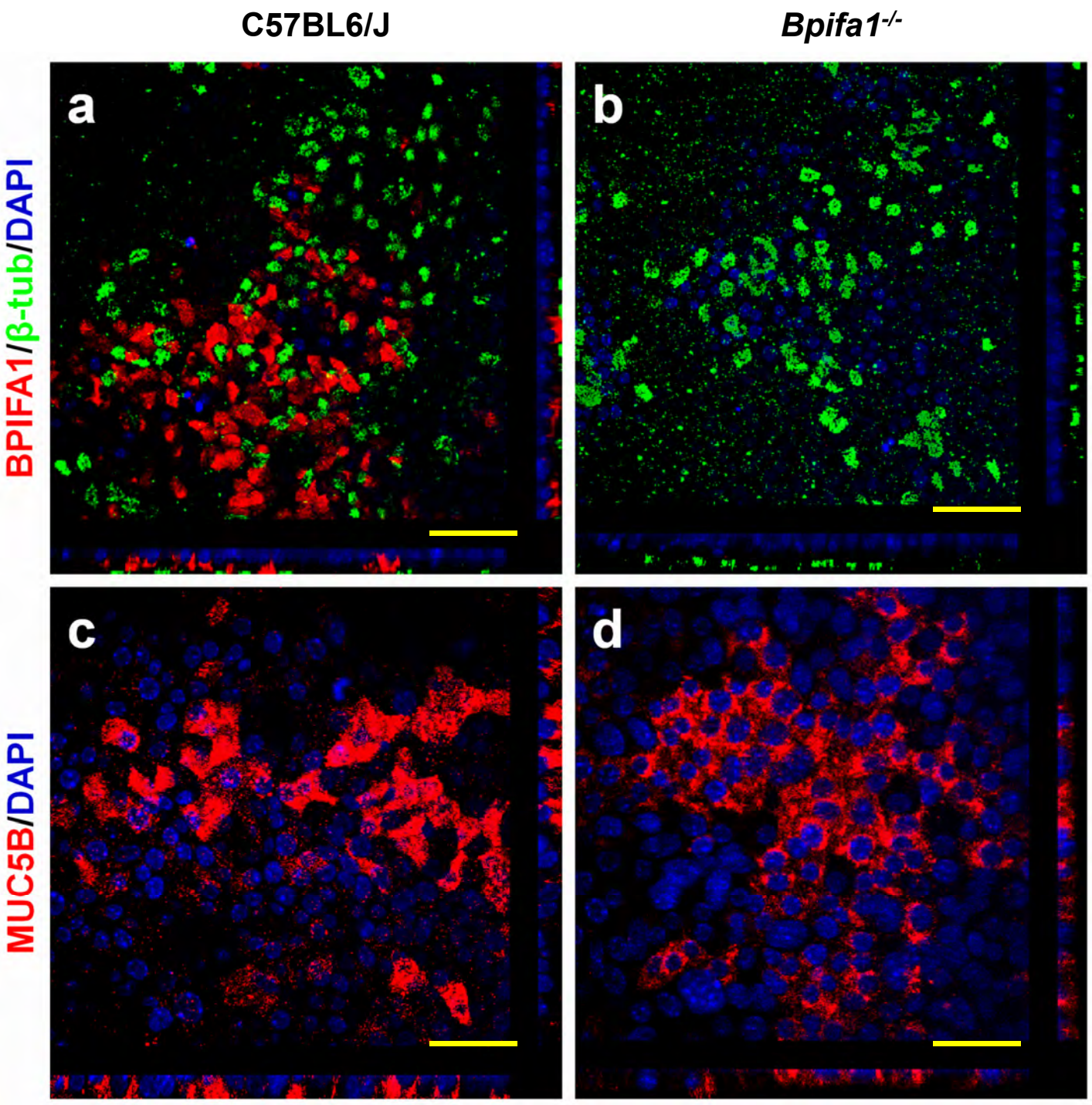

S5 Fig

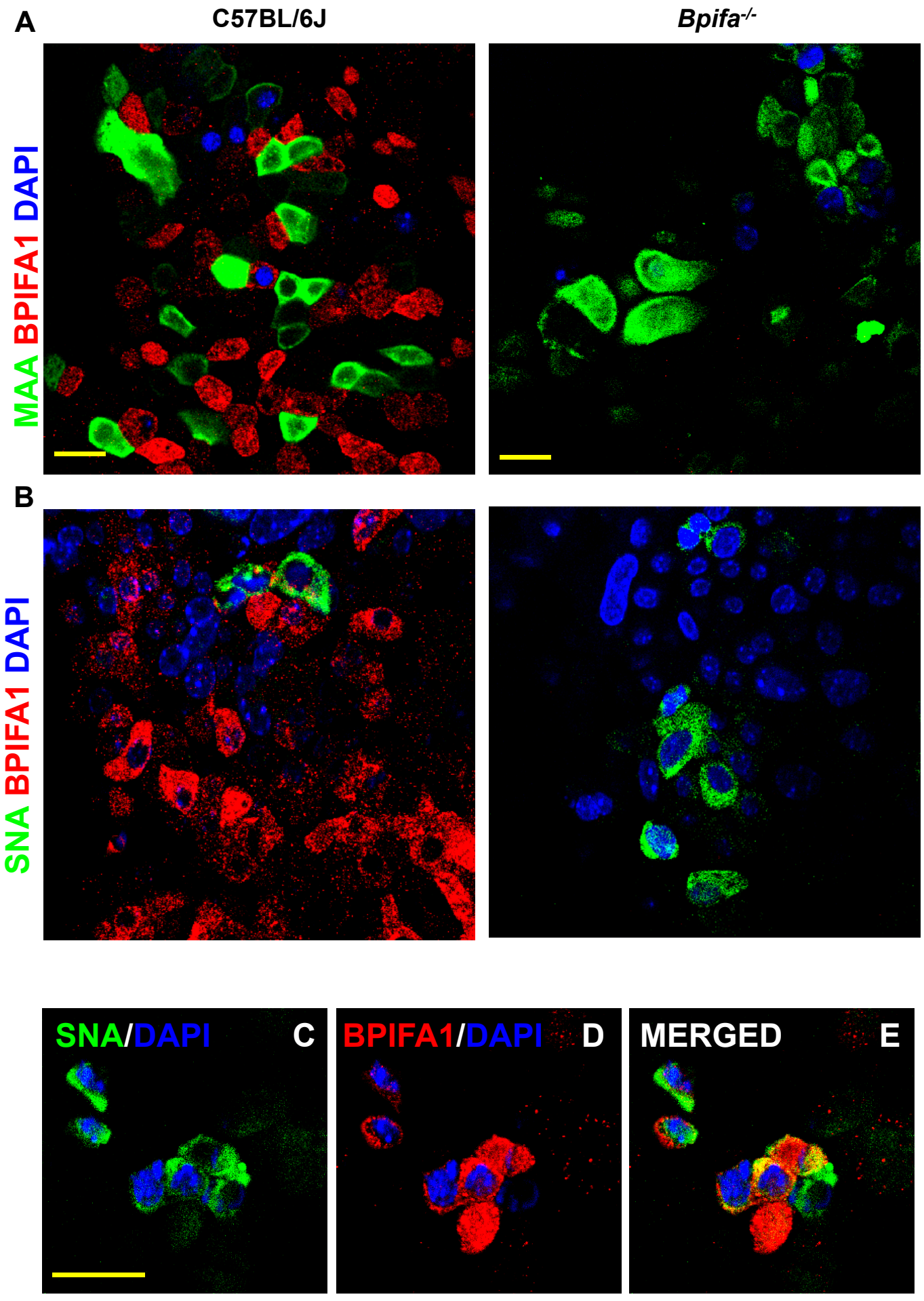
A
C57BL/6J
Bpifa-/-
MAA BPIFA1 DAPI
B
SNA BPIFA1 DAPI
SNA/DAPI
C
BPIFA1/DAPI
D
MERGED
E